

## Sandy coastlines under threat of erosion

Vousdoukas, Michalis I.; Ranasinghe, Roshanka; Mentaschi, Lorenzo; Plomaritis, Theocharis A.; Athanasiou, Panagiotis; Luijendijk, Arjen; Feyen, Luc

**DOI**

[10.1038/s41558-020-0697-0](https://doi.org/10.1038/s41558-020-0697-0)

**Publication date**

2020

**Document Version**

Accepted author manuscript

**Published in**

Nature Climate Change

**Citation (APA)**

Vousdoukas, M. I., Ranasinghe, R., Mentaschi, L., Plomaritis, T. A., Athanasiou, P., Luijendijk, A., & Feyen, L. (2020). Sandy coastlines under threat of erosion. *Nature Climate Change*, 10(3), 260-263.  
<https://doi.org/10.1038/s41558-020-0697-0>

**Important note**

To cite this publication, please use the final published version (if applicable).  
Please check the document version above.

**Copyright**

Other than for strictly personal use, it is not permitted to download, forward or distribute the text or part of it, without the consent of the author(s) and/or copyright holder(s), unless the work is under an open content license such as Creative Commons.

**Takedown policy**

Please contact us and provide details if you believe this document breaches copyrights.  
We will remove access to the work immediately and investigate your claim.

# 1. Extended Data

Figure #	Figure title  One sentence only	Filename  This should be the name the file is saved as when it is uploaded to our system. Please include the file extension. i.e.:  <i>Smith_ED_Fi_1.jpg</i>	Figure Legend  If you are citing a reference for the first time in these legends, please include all new references in the Online Methods References section, and carry on the numbering from the main References section of the paper.
Extended Data Fig. 1	Geographical regions considered in the present analysis	Vousdoukas_ED_01.eps	Geographical regions considered in the present analysis, based on the IPCC SREX report and limited to those that contain ice-free sandy coastlines
Extended Data Fig. 2	Projected long term shoreline change due to SLR driven retreat (R) alone, by the year 2050 and 2100 under RCP4.5 and RCP8.5.	Vousdoukas_ED_02.eps	Projected long term shoreline change due to SLR driven retreat (R) alone, by the year 2050 (a,c) and 2100 (b,d) under RCP4.5 (a-b) and RCP8.5 (c-d). Values represent the median change and positive/negative values express accretion/erosion in m, relative to 2010. The global average median change is shown in the inset text for each case, along with the 5 <sup>th</sup> -95 <sup>th</sup> percentile range.
Extended Data Fig. 3	Projected long term shoreline change driven due to the ambient shoreline change rate (AC) alone, by the year 2050 and 2100.	Vousdoukas_ED_03.eps	Projected long term shoreline change driven due to the ambient shoreline change rate (AC) alone, by the year 2050 (a) and 2100 (b). Values represent the median change and positive/negative values express accretion/erosion in m, relative to 2010. The global average median change is shown in the inset text for each case, along with the 5 <sup>th</sup> -95 <sup>th</sup> percentile range.
Extended Data Fig. 4	Projected change in 100-year episodic beach erosion for the year 2050 and 2100 under RCP4.5 and	Vousdoukas_ED_04.eps	Projected change in 100-year episodic beach erosion for the year 2050 (a,c) and 2100 (b,d) under RCP4.5 (a-b) and RCP8.5 (c-d). Values represent the median change and positive/negative values express less/more erosion (m), relative to 2010. The global average median change is shown in

	RCP8.5.		the inset text for each case, along with the 5 <sup>th</sup> -95 <sup>th</sup> percentile range.
Extended Data Fig. 5	Projected median long term shoreline change under RCP4.5 by the year 2050 ( $dx_{shore,LT}$ ), for the 26 IPCC SREX sub- regions and the worldwide average	Vousdoukas_ED_05.eps	Projected median long term shoreline change under RCP4.5 by the year 2050 ( $dx_{shore,LT}$ ), for the 26 IPCC SREX sub- regions and the worldwide average (horizontal bar plot; positive/negative values express accretion/erosion in m). Shoreline change is considered to be the result of SLR retreat (R) and ambient shoreline change trends (AC). Pie plots show the relative contributions of R and AC to the projected median $dx_{shore,LT}$ , with transparent patches expressing accretive trends. Vertical bar plots show the relative contributions of R and AC, as well as that of RCPs, to the total uncertainty in projected median $dx_{shore,LT}$ .
Extended Data Fig. 6	Projected median long term shoreline change under RCP8.5 by the year 2050 ( $dx_{shore,LT}$ ), for the 26 IPCC SREX sub- regions and the worldwide average	Vousdoukas_ED_06.eps	Projected median long term shoreline change under RCP8.5 by the year 2050 ( $dx_{shore,LT}$ ), for the 26 IPCC SREX sub- regions and the worldwide average (horizontal bar plot; positive/negative values express accretion/erosion in m). Shoreline change is considered to be the result of SLR retreat (R) and ambient shoreline change trends (AC). Pie plots show the relative contributions of R and AC to the projected median $dx_{shore,LT}$ , with transparent patches expressing accretive trends. Vertical bar plots show the relative contributions of R and AC, as well as that of RCPs, to the total uncertainty in projected median $dx_{shore,LT}$ .
Extended Data Fig. 7	Projected median long term shoreline change under RCP4.5 by the year 2100 ( $dx_{shore,LT}$ ), for the 26 IPCC SREX sub- regions and the worldwide average	Vousdoukas_ED_07.eps	Projected median long term shoreline change under RCP4.5 by the year 2100 ( $dx_{shore,LT}$ ), for the 26 IPCC SREX sub- regions and the worldwide average (horizontal bar plot; positive/negative values express accretion/erosion in m). Shoreline change is considered to be the result of SLR retreat (R) and ambient shoreline change trends (AC). Pie plots show the relative contributions of R and AC to the projected

			median $dx_{shore,LT}$ with transparent patches expressing accretive trends. Vertical bar plots show the relative contributions of R and AC, as well as that of RCPs, to the total uncertainty in projected median $dx_{shore,LT}$ .
Extended Data Fig. 8	Percentage length of sandy beach shoreline that is projected to retreat by more than 50, 100 and 200 m per IPCC SREX sub-region	Vousdoukas_ED_08.eps	Bar plots showing, per IPCC SREX sub-region, the percentage length of sandy beach shoreline that is projected to retreat by more than 50 (blue), 100 (yellow) and 200 m (red), by 2050 (a,c) and 2100 (b,d), under RCP4.5 (a-b) and RCP8.5 (c-d) relative to 2010. Transparent color patches indicate the 5 <sup>th</sup> -95 <sup>th</sup> quantile range and solid rectangles show the median value. For the region abbreviations, please see Extended Data Fig. 1.
Extended Data Fig. 9	Length of sandy beach shoreline that is projected to retreat by more than 50, 100 and 200 m per IPCC SREX sub-region	Vousdoukas_ED_09.eps	Bar plots showing, per IPCC SREX sub-region, the length (in km) of sandy beach shoreline that is projected to retreat by more than 50 (blue), 100 (yellow) and 200 m (red), by 2050 (a,c) and 2100 (b,d), under RCP4.5 (a-b) and RCP8.5 (c-d) relative to 2010. Transparent color patches indicate the 5 <sup>th</sup> -95 <sup>th</sup> quantile range and solid rectangles show the median value. For the region abbreviations, please see Supplementary Figs. S2 and S5
Extended Data Fig. 10	Per country length of sandy beach shoreline that is projected to retreat by more than 100 m	Vousdoukas_ED_10.eps	Per country length of sandy beach coastline which is projected to retreat by more than 100 m by 2050 (a,c) and 2100 (b,d), under RCP4.5 (a-b) and RCP8.5 (c-d). Values are based on the median long term shoreline change, relative to 2010.

## 2. Supplementary Information:

### A. Flat Files

Item	Present?	Filename	A brief, numerical description of file contents.
		This should be the	

		name the file is saved as when it is uploaded to our system, and should include the file extension. The extension must be .pdf	i.e.: <i>Supplementary Figures 1-4, Supplementary Discussion, and Supplementary Tables 1-4.</i>
Supplementary Information	Yes	Vousdoukas_NLetter_SI.pdf	<i>Supplementary Figure 1, Supplementary Tables 1-4.</i>
Reporting Summary	Choose an item.		

## B. Additional Supplementary Files

Type	Number  If there are multiple files of the same type this should be the numerical indicator. i.e. "1" for Video 1, "2" for Video 2, etc.	Filename  This should be the name the file is saved as when it is uploaded to our system, and should include the file extension. i.e.: <i>Smith_Supplementary_Video_1.mov</i>	Legend or Descriptive Caption  Describe the contents of the file
Choose an item.			
Choose an item.			
Choose an item.			
Choose an item.			
Choose an item.			
Choose an item.			

## 3. Source Data

Parent Figure or Table	Filename  This should be the name the file is saved as when it is uploaded to	Data description  e.g.: Unprocessed Western Blots and/or gels,
------------------------	---	--

	our system, and should include the file extension. i.e.: <i>Smith_SourceData_Fig1.xls</i> , or <i>Smith_Unmodified_Gels_Fig1.pdf</i>	Statistical Source Data, etc.
Source Data Fig. 1		
Source Data Fig. 2		
Source Data Fig. 3		
Source Data Fig. 4		
Source Data Fig. 5		
Source Data Fig. 6		
Source Data Fig. 7		
Source Data Fig. 8		
Source Data Extended Data Fig. 1		
Source Data Extended Data Fig. 2		
Source Data Extended Data Fig. 3		
Source Data Extended Data Fig. 4		
Source Data Extended Data Fig. 5		

Source Data Extended Data Fig. 6		
Source Data Extended Data Fig. 7		
Source Data Extended Data Fig. 8		
Source Data Extended Data Fig. 9		
Source Data Extended Data Fig. 10		

14

15

16

## Sandy coastlines under threat of erosion

17

Michalis I. Vousdoukas<sup>1\*</sup>, Roshanka Ranasinghe<sup>2,3,4</sup>, Lorenzo Mentaschi<sup>1</sup>, Theocharis A. Plomaritis<sup>5,6</sup>,

18

Panagiotis Athanasiou<sup>3,4</sup>, Arjen Luijendijk<sup>4,7</sup>, Luc Feyen<sup>1</sup>

19

<sup>1</sup> European Commission, Joint Research Centre (JRC), Email: [Michail.VOUSDOKAS@ec.europa.eu](mailto:Michail.VOUSDOKAS@ec.europa.eu); Tel:

20

+39 033278-6499; Fax: +39 033278-665

21

<sup>2</sup> Department of Water Science and Engineering, IHE Delft Institute for Water Education, PO Box 3015,

22

2610 DA Delft, the Netherlands

23

<sup>3</sup> Water Engineering and Management, Faculty of Engineering Technology, University of Twente, PO, Box

24

217, 7500 AE Enschede, the Netherlands

25

<sup>4</sup> Harbour, Coastal and Offshore Engineering, Deltares, PO Box 177, 2600 MH Delft, the Netherlands

26

<sup>5</sup> University of Cadiz, Dpt. Applied Physics, CASEM, University of Cadiz, 11510 Puerto Real, Cádiz, Spain

27

<sup>6</sup> CIMA, University of Algarve, Campus de Gambelas, 8005-139, Faro, Portugal

28

<sup>7</sup> Faculty of Civil Engineering and Geosciences, Department of Hydraulic Engineering, Delft University of

29

Technology, P.O. Box 5048, 2600 GA Delft, The Netherlands

\*Corresponding author address:

Dr Michalis Vousdoukas

European Commission, Joint European Research Centre (JRC), Via Enrico Fermi 2749, I-21027, Ispra, Italy. Email: [Michail.VOUSDOKAS@ec.europa.eu](mailto:Michail.VOUSDOKAS@ec.europa.eu); Tel: +39 033278-6499; Fax: +39 033278-665

**Sandy beaches occupy more than one third of the global coastline<sup>1</sup> and have high socio-economic value related to recreation, tourism, and ecosystem services<sup>2</sup>. Beaches are the interface between land and ocean, providing coastal protection from marine storms and cyclones<sup>3</sup>. However the presence of sandy beaches cannot be taken for granted, as they are under constant change, driven by meteorological<sup>4,5</sup>, geological<sup>6</sup>, and anthropogenic factors<sup>1,7</sup>. A substantial proportion of the world's sandy coastline is already eroding<sup>1,7</sup>, a situation that could be exacerbated by climate change<sup>8,9</sup>. Here, we show that with, climate mitigation, ambient trends in shoreline dynamics, combined with coastal recession driven by sea level rise could result in the near extinction of almost half of the world's sandy beaches by the end of the century. Moderate greenhouse gas emission mitigation could prevent 40% of shoreline retreat. Projected shoreline dynamics are dominated by sea level rise for the majority of sandy beaches, but in certain regions this is overshadowed by ambient shoreline changes. In West and East Asia, long-term accretion up to 200-300 m is projected. A significant proportion of the threatened sandy shorelines are in densely populated areas, underlining the need for the design and implementation of effective adaptive measures.**

The coastal zone is among the most developed areas worldwide, containing an abundance of developments, critical infrastructure<sup>10</sup>, and ecosystems<sup>2,3</sup>. As a result, population density tends to be higher near the coast<sup>11</sup>, and most projections indicate that current trends of coastward migration, urbanization and population growth will continue<sup>12,13</sup>. Of the different beach typologies found worldwide sandy beaches are the most heavily utilized<sup>14</sup> and are among the most geomorphologically complex, with the shoreline, i.e. the mean water line along the coast, changing constantly under forcing-response interactions between natural and anthropogenic factors<sup>7</sup>.



The global mean sea level has been increasing at an accelerated rate during the past 25 years<sup>15</sup> and will continue to do so in view of climate change<sup>16,17</sup>. While shoreline change can be the combined result of a wide range of potentially erosive or accretive factors<sup>8</sup>, there is a clear cause and effect relation between increasing sea levels and shoreline retreat<sup>18</sup>, pointing to increased coastal erosion issues<sup>9,19</sup>. Climate change will also affect waves and storm surges<sup>20,21</sup>, which are important drivers of coastal morphology<sup>4,5,22</sup>, and therefore considering the dynamics of extreme weather patterns is also important in assessing potential climate change impacts beyond that of SLR alone.

Here we present a comprehensive global analysis of sandy shoreline dynamics during the 21<sup>st</sup> century. Our probabilistic projections explicitly take into account estimates of future SLR, spatial variations of coastal morphology, ambient shoreline change trends, and future changes in meteorological drivers (e.g. storm surge and waves). We first evaluate long term shoreline change  $dx_{shore\_LT}$ , which is the result of two components: the ambient shoreline change (AC) driven by geological, anthropogenic and other physical factors<sup>7</sup> and the shoreline retreat due to SLR ( $R$ ) (Supplementary Fig. S1). We obtained AC by extrapolating observed historical trends<sup>7</sup> within a probabilistic framework (see Methods). We computed  $R$  by using a modified Bruun rule<sup>18</sup> together with a new global dataset of active beach slopes<sup>23</sup>. In addition to the long term shoreline dynamics we also project how maximum erosion from coastal storms may change in view of climate change. Shoreline change projections are discussed for the years 2050 and 2100 under RCP 4.5 and 8.5, relative to the baseline year 2010.

Our analysis shows an overall erosive trend of sandy beaches that increases in time and with the intensity of greenhouse gas emissions (Figure 1). Assuming that there are no physical limits in potential retreat, by mid-century we project a very likely (5-95<sup>th</sup> percentile) global average long term shoreline change  $dx_{shore\_LT}$  ranging from -2.2 to -79.2 m and -0.8 to -99.2 m, under RCP4.5 and RCP8.5, respectively (negative values express erosion; Supplementary Table S1). By the end of the century the erosive trend becomes even more dominant and we project a very likely range from -21.7 to -171.1 m and -42.2 to -246.9 m under RCP4.5 and RCP8.5, respectively (Figure 2 Supplementary Table S1). Moderate greenhouse gas emission mitigation could thus prevent 22% of the projected shoreline retreat by 2050 and 40% by the end of the century (Supplementary Table S1). This corresponds to a global average of around 42 m of preserved sandy beach width by the end of the century.

The global erosive trend masks high spatial variability, with erosive and accretive tendencies interchanging across regions and along nearby coastal segments (Figure 1). Whereas local trends can exceed several meters per year, eight IPCC sub-regions show median retreats exceeding 100 m under

both RCPs by the end of the century (Supplementary Table S1; see Figure 2 for a definition of the regions): East North America, Amazon, Southeastern South America, Central Europe, South and West Asia, North Australia, and the Caribbean SIDS. By 2100,  $dx_{shore,LT}$  exceeds 150 m under RCP8.5 in all the above regions, while under the same scenario median retreats larger than 300 m are projected for South Asia and the Caribbean SIDS. Long term accretion is projected along sandy coastlines of East Asia under both RCPs by 2050 and only under RCP4.5 by the end of the century.

SLR driven retreat  $R$  is responsible for 71% and 75% of the global median shoreline change in 2050 under RCP4.5 and RCP8.5, respectively (Extended data Figs 5-6); and for 86% and 77% by the end of the century (Figure 2 and Extended Data Fig. 7). Ambient shoreline changes dominate only in certain regions, in particular in South and West Asia, West Indian Ocean, Southeastern South America, and the Caribbean SIDS regions. The contributions of the SLR retreat and ambient change to the overall uncertainty under RCP4.5 and by mid-century are relatively balanced (Extended Data Fig. 5), while AC contributes to 41% more uncertainty globally, by the end of the century (Extended Data Fig. 7). Under RCP8.5 uncertainty related to SLR retreat dominates that of AC, by 44% and 30%, by the years 2050 and 2100, respectively (Extended Data Fig. 7 and Figure 2). Regionally, ambient change uncertainty is higher in North Australia South Asia.

The above estimates do not include the episodic, storm-driven shoreline retreat  $S$ , presently projected using the convolution erosion model of Kriebel and Dean<sup>24</sup> (see Methods). Here we discuss the 100-year event  $S$  which for the year 2050 is equivalent to circa 23% of the global average projected long term shoreline change  $dx_{shore,LT}$  (Supplementary Tables S1-4). By the end of the 21<sup>st</sup> century, the relative importance of the 100-year  $S$  compared to  $dx_{shore,LT}$  decreases to 9% and 7% under RCP4.5 and 8.5, respectively, as long term changes gather pace. Storm erosion is typically followed by beach recovery<sup>25</sup>, but some events may leave a footprint that takes decades to recover, if at all<sup>4,26</sup>, while the additional shoreline retreat renders the backshore more vulnerable to episodic coastal flooding and its consequences. Despite previous studies projecting changes in wave intensity and direction worldwide<sup>21,27,28</sup>, our projections show that overall climate change will not have a strong effect on episodic storm driven erosion. As a result, ambient and SLR driven change appear to shadow the effect of changes in storm-driven erosion, even though at certain locations  $\Delta S$  values can reach  $\pm 20$  m by the end of the century; e.g. increase in 100-year erosion potential along the South East UK, West coast of Germany, North Queensland (Australia), and Acapulco (Mexico) (Extended Data Fig. 4).

The projected shoreline changes will substantially impact on the shape of the world's coastline. Many coastal systems have lost already their natural capacity to accommodate or recover from erosion, as the backshore is heavily occupied by human settlements<sup>29</sup>, while dams and human development have depleted terrestrial sediment supply which would naturally replenish the shore with new material<sup>30,31</sup>. Most of the remaining regions with an extensive presence of a natural coastline, are found in Africa and Asia, which are also the regions projected to experience the highest coastal population and urbanization growth in the decades to come<sup>12,13</sup>. There is yet no global dataset on sandy beach width allowing to accurately estimate the potential loss of sandy beaches around the world. Therefore, to quantify the potential impact of our projections, we consider beaches that are projected to experience a shoreline retreat >100 m as seriously threatened by coastal erosion. The chosen 100 m threshold is rather conservative, since most sandy beaches have widths below 50 m, especially near human settlements, small islands and micro-tidal areas (e.g. Caribbean, Mediterranean).

We find that 10.6%-12.2% (28,260-32,456 km) of the world's sandy beaches could face severe erosion by 2050 and 37.2%-50.9% (99,996-135,279 km) by the end of the century (Extended Data Fig. 8). Thirty one percent (31%) of the world's sandy beaches are in low elevation coastal zones (LECZ) with population density exceeding 500 people per km<sup>2</sup>, and our projections show that approximately one third of these LECZ sandy coasts will be seriously threatened by erosion by the year 2050. This estimate reaches 51% and 62% by the end of the century, under RCP4.5 and RCP8.5, respectively.

Several countries could face extensive erosion by the end of the 21<sup>st</sup> century (along >80% of their sandy coastline under both RCPs; Figure 3) including Democratic Republic of the Congo, Gambia, Jersey, Suriname, Comoros, Palau, Benin, Guinea-Bissau, Mayotte, Iraq, Pakistan, Guinea and El Salvador. Apart from the consequent higher vulnerability to coastal hazards, several of these countries are likely to experience substantial socioeconomic implications as their economies are fragile and, tourism-dependent with sandy coastlines constituting their major tourist attraction. When the total length of sandy beaches projected to be lost by 2100 is considered (as opposed to the %), Australia emerges as the potentially most affected country, with at least 12,324 km of sandy beach coastline threatened by erosion (15,439 under RCP8.5; Extended Data Fig. 9), circa 40% of the country's total sandy coastline. By the same impact metric, Canada ranks second (9,577 and 16,651 km 15,439 under RCP4.5 and RCP8.5, respectively), followed by Chile (5,471 and 7,050 km), Mexico (4,119 and 5,105 km) China (4,084 and 5,185 km), USA (3,908 and 5,553 km), Argentina (3,668 and 4,413 km) and Iran (3,654 and 3,870 km).

Past experience has shown that effective site-specific coastal planning can mitigate beach erosion, eventually resulting in a stable coastline; with the most prominent example being the Dutch coast<sup>32</sup>. A positive message from the present analysis is that while SLR will drive shoreline retreat almost everywhere, many locations show ambient erosive trends related to human interventions<sup>7</sup>, which in theory could be avoided by more sustainable coastal zone and catchment management practices. At the same time, the range of projected SLR implies unprecedented pressure to our coasts which requires the development and implementation of informed and effective adaptive measures.

## CORRESPONDENCE

Correspondence and requests for materials should be addressed to M.I.V.

## References

- 1 Luijendijk, A. *et al.* The State of the World's Beaches. *Scientific Reports* **8**, 6641, doi:10.1038/s41598-018-24630-6 (2018).
- 2 Barbier, E. B. *et al.* The value of estuarine and coastal ecosystem services. *Ecological Monographs* **81**, 169-193, doi:10.1890/10-1510.1 (2011).
- 3 Temmerman, S. *et al.* Ecosystem-based coastal defence in the face of global change. *Nature* **504**, 79, doi:10.1038/nature12859 (2013).
- 4 Masselink, G. *et al.* Extreme wave activity during 2013/2014 winter and morphological impacts along the Atlantic coast of Europe. *Geophys. Res. Lett.* **43**, 2135-2143, doi:10.1002/2015GL067492 (2016).
- 5 Barnard, P. L. *et al.* Coastal vulnerability across the Pacific dominated by El Nino/Southern Oscillation. *Nat. Geosci.* **8**, 801-807, doi:10.1038/ngeo2539 (2015).
- 6 Cooper, J. A. G., Green, A. N. & Loureiro, C. Geological constraints on mesoscale coastal barrier behaviour. *Global Planet. Change* **168**, 15-34, doi:https://doi.org/10.1016/j.gloplacha.2018.06.006 (2018).
- 7 Mentaschi, L., Vousdoukas, M. I., Pekel, J.-F., Voukouvalas, E. & Feyen, L. Global long-term observations of coastal erosion and accretion. *Scientific Reports* **8**, 12876, doi:10.1038/s41598-018-30904-w (2018).
- 8 Ranasinghe, R. Assessing climate change impacts on open sandy coasts: A review. *Earth-Science Reviews* **160**, 320-332, doi:https://doi.org/10.1016/j.earscirev.2016.07.011 (2016).
- 9 Hinkel, J. *et al.* A global analysis of erosion of sandy beaches and sea-level rise: An application of DIVA. *Global Planet. Change* **111**, 150-158, doi:https://doi.org/10.1016/j.gloplacha.2013.09.002 (2013).
- 10 Koks, E. E. *et al.* A global multi-hazard risk analysis of road and railway infrastructure assets. *Nature Communications* **10**, 2677, doi:10.1038/s41467-019-10442-3 (2019).
- 11 McGranahan, G., Balk, D. & Anderson, B. The rising tide: assessing the risks of climate change and human settlements in low elevation coastal zones. *Environment and Urbanization* **19**, 17-37, doi:10.1177/0956247807076960 (2007).
- 12 Neumann, B., Vafeidis, A. T., Zimmermann, J. & Nicholls, R. J. Future Coastal Population Growth and Exposure to Sea-Level Rise and Coastal Flooding - A Global Assessment. *PLOS ONE* **10**, e0118571, doi:10.1371/journal.pone.0118571 (2015).

189 13 Jones, B. & O'Neill, B. C. Spatially explicit global population scenarios consistent with the Shared  
190 Socioeconomic Pathways. *Environmental Research Letters* **11**, doi:10.1088/1748-  
191 9326/11/8/084003 (2016).

192 14 Davenport, J. & Davenport, J. L. The impact of tourism and personal leisure transport on coastal  
193 environments: A review. *Estuar. Coast. Shelf Sci.* **67**, 280-292,  
194 doi:https://doi.org/10.1016/j.ecss.2005.11.026 (2006).

195 15 Nerem, R. S. *et al.* Climate-change-driven accelerated sea-level rise detected in the altimeter  
196 era. *Proceedings of the National Academy of Sciences* **115**, 2022-2025,  
197 doi:10.1073/pnas.1717312115 (2018).

198 16 Bamber, J. L., Oppenheimer, M., Kopp, R. E., Aspinall, W. P. & Cooke, R. M. Ice sheet  
199 contributions to future sea-level rise from structured expert judgment. *Proceedings of the*  
200 *National Academy of Sciences*, 201817205, doi:10.1073/pnas.1817205116 (2019).

201 17 Jevrejeva, S., Jackson, L. P., Riva, R. E. M., Grinsted, A. & Moore, J. C. Coastal sea level rise with  
202 warming above 2 °C. *Proceedings of the National Academy of Sciences* **113**, 13342-13347,  
203 doi:10.1073/pnas.1605312113 (2016).

204 18 Bruun, P. Sea level rise as a cause of shore erosion. *Journal of Waterway, Harbors Division. ASCE*  
205 **88**, 117 (1962).

206 19 Anthony, E. J. *et al.* Linking rapid erosion of the Mekong River delta to human activities.  
207 *Scientific Reports* **5**, 14745, doi:10.1038/srep14745 (2015).

208 20 Vousdoukas, M. I. *et al.* Global probabilistic projections of extreme sea levels show  
209 intensification of coastal flood hazard. *Nature Communications* **9**, 2360, doi:10.1038/s41467-  
210 018-04692-w (2018).

211 21 Hemer, M. A., Fan, Y., Mori, N., Semedo, A. & Wang, X. L. Projected changes in wave climate  
212 from a multi-model ensemble. *Nature Clim. Change* **3**, 471-476, doi:10.1038/nclimate1791  
213 (2013).

214 22 Slott, J. M., Murray, A. B., Ashton, A. D. & Crowley, T. J. Coastline responses to changing storm  
215 patterns. *Geophys. Res. Lett.* **33**, doi:10.1029/2006GL027445 (2006).

216 23 Athanasiou, P. *et al.* A global dataset of coastal slopes for coastal recession assessments. *Earth*  
217 *System Science Data Discussions* **11**, 1515–1529, doi:https://doi.org/10.5194/essd-11-1515-  
218 2019 (2019).

219 24 Kriebel, D. L. & Dean, R. G. Convolution method for time dependent beach profile response.  
220 *Journal of Waterway, Port, Coastal and Ocean Engineering* **119**, 204-226 (1993).

221 25 Vousdoukas, M. I. Erosion/accretion patterns and multiple beach cusp systems on a meso-tidal,  
222 steeply-sloping beach. *Geomorphology* **141**, 34-46, doi:10.1016/j.geomorph.2011.12.003 (2012).

223 26 Anderson, T. R., Frazer, L. N. & Fletcher, C. H. Transient and persistent shoreline change from a  
224 storm. *Geophys. Res. Lett.* **37**, doi:10.1029/2009gl042252 (2010).

225 27 Erikson, L. H., Hegermiller, C. A., Barnard, P. L., Ruggiero, P. & van Ormondt, M. Projected wave  
226 conditions in the Eastern North Pacific under the influence of two CMIP5 climate scenarios.  
227 *Ocean Modelling* **96**, 171-185, doi:https://doi.org/10.1016/j.ocemod.2015.07.004 (2015).

228 28 Mentaschi, L., Vousdoukas, M. I., Voukouvalas, E., Dosio, A. & Feyen, L. Global changes of  
229 extreme coastal wave energy fluxes triggered by intensified teleconnection patterns. *Geophys.*  
230 *Res. Lett.* **44**, 2416-2426, doi:10.1002/2016GL072488 (2017).

231 29 Small, C. & Nicholls, R. J. A Global Analysis of Human Settlement in Coastal Zones. *J. Coast. Res.*  
232 **19**, 584-599 (2003).

233 30 Milliman, J. D. Blessed dams or damned dams? *Nature* **386**, 325-327, doi:10.1038/386325a0  
234 (1997).

235 31 Ranasinghe, R., Wu, C. S., Conallin, J., Duong, T. M. & Anthony, E. J. Disentangling the relative  
236 impacts of climate change and human activities on fluvial sediment supply to the coast by the  
237 world's large rivers: Pearl River Basin, China. . *Scientific Reports* (accepted).  
238 32 Brière, C., Janssen, S. K. H., Oost, A. P., Taal, M. & Tonnon, P. K. Usability of the climate-resilient  
239 nature-based sand motor pilot, The Netherlands. *J. Coast. Conserv.* **22**, 491-502,  
240 doi:10.1007/s11852-017-0527-3 (2018).  
241

## Figure captions

*Figure 1. Projected long term shoreline change. By the year 2050 (a,c) and 2100 (b,d) under RCP4.5 (a-b) and RCP8.5 (c-d). Values represent the median change and positive/negative values respectively express accretion/erosion in m, relative to 2010. The global average median change is shown in the inset text for each case, along with the 5th-95th percentile range.*

*Figure 2. Projected median long term shoreline change under RCP8.5 by the year 2100 ( $dx_{shore,LT}$ ), for the 26 IPCC SREX sub-regions and the worldwide average. For the horizontal bar plot on right; positive/negative values express accretion/erosion in m; black error bars indicate the 5<sup>th</sup>-95<sup>th</sup> quantile range. Shoreline change is considered to be the result of SLR retreat (R) and ambient shoreline change trends (AC). Pie plots show the relative contributions of R and AC to the projected median  $dx_{shore,LT}$ , with transparent slices expressing accretive trends. Vertical bar plots show the ratio between the uncertainty of R and AC (5<sup>th</sup>-95<sup>th</sup> quantile range), to the total uncertainty in projected median  $dx_{shore,LT}$ .*

*Figure 3. Per country percentages of the sandy coastline length which is projected to retreat by more than 100 m. By 2050 (a,c) and 2100 (b,d), under RCP4.5 (a-b) and RCP8.5 (c-d). Values are based on the median long term shoreline change, relative to 2010.*

# 1 Methods

## 1.1 General concepts

In this study we project shoreline dynamics throughout this century along the world's sandy coastlines under two Representative Concentration Pathways (RCPs): RCP4.5 and RCP8.5. RCP4.5 may be viewed as a *moderate-emission-mitigation-policy scenario* and RCP8.5 as a *high-emissions scenario*<sup>33</sup>. The study focusses on the evolution of three components of sandy beach shoreline dynamics (Supplementary Fig. S1):

- AC: Ambient shoreline dynamics driven by long-term hydrodynamic, geological and anthropic factors.
- R: Shoreline retreat due to coastal morphological adjustments to Sea Level Rise (SLR).
- S: Episodic erosion during extreme storms.

The first two components represent longer term shoreline changes and are quantified here as:

$$dx_{shore,LT} = AC + R \quad 1$$

AC expresses long-term ambient shoreline dynamics that can be driven by a wide range of natural and/or anthropogenic processes, excluding the effect of SLR ( $R$ ) and that of episodic erosion during extreme events ( $S$ ; see following paragraph). In most cases AC is related to human interventions that alter the sediment budget and/or transport processes of coastal systems<sup>7</sup>, but it also includes natural transitions due to a variety of reasons, such as weather patterns<sup>4,34-36</sup>, persistent longshore transport variations<sup>37</sup>, or geological control<sup>38,39</sup>.  $R$  in Eq. 1 represents SLR-driven shoreline retreat, the magnitude of which depends on the transfer of sediment from the sub-aerial to the submerged part of the active beach profile, in order to adjust to rising Mean Sea Levels (MSLs).

The third component  $S$  represents episodic erosion from intense waves and storm surges during extreme weather events. Episodic erosion is usually followed by a recovery process<sup>40-42</sup>. It is assumed here that the irreversible net effect of episodic erosion and post-storm recovery constitutes part of the ambient shoreline evolution expressed by AC.  $S$  is therefore limited to the reversible episodic shoreline retreat during storm events relative to its long term position expressed by  $dx_{shore,LT}$ . Potential variations in storminess with global warming will induce changes in  $S$  compared to present day conditions.



At any point in time, the maximum shoreline retreat  $dx_{shore,max}$  during an extreme coastal event due to the combined effects of long-term and episodic erosion is then defined as

$$dx_{shore,max} = AC + R + S \quad 2$$

Each of these components are discussed in more detail below.

This study focuses on ice-free sandy beaches, which constitute the most common and dynamic beach type globally, covering more than 30% of the ice-free coastline in the world<sup>1,43</sup>. While in reality shoreline retreat can be limited by the presence of natural or anthropogenic barriers, spatial data on such features is not available globally at the resolution needed for the present study. Adaptive measures against beach erosion could have a similar effect, but are difficult to predict and merit a separate study. Therefore, we do not invoke any physical limits to the extent of potential shoreline retreat.

## 1.2 Ambient shoreline dynamics

Several parts of the global coastline undergo long-term ambient changes as a result of various hydrodynamic, geological and anthropic factors. Historical shoreline trends were estimated by Mentaschi et al.<sup>7</sup> from the high-resolution Global Surface Water (GSW) database<sup>44</sup>. It provides spatio-temporal dynamics of surface water presence globally at 30 m resolution from 1984 to 2015, obtained by the automated analysis of over 3 million Landsat satellite images. This GSW dataset was processed for changes in water presence in coastal areas to produce time series of cross-shore shoreline position<sup>7</sup>. The pixel-wise information of GSW was translated into cross-shore shoreline dynamics using a set of over 2,000,000 shore-normal transects. The transects were defined every 250 m along a global coastline obtained from OpenStreetMap<sup>45</sup> and were sufficiently long to accommodate the shoreline displacement during the study period. Each transect defines a 200 m alongshore-wide coastal section, along which surface water transitions were considered in order to extract time-series of shoreline displacement along each shore normal transect.

We consider as a proxy for the shoreline change the cross-shore displacement of the seaward boundary of the ‘permanent land layer’; i.e. the areas where water presence has never been detected throughout the year. Over the 32-year period considered, the selected proxy can respond to tidal, storm surge, wave and swash dynamics, as well as the inter-related dynamics of the beach face slope or nearshore bathymetry. Among the different shoreline definitions proposed in literature<sup>46</sup>, the present one was chosen as it is more compatible with the type of analysis and the spatial and temporal resolution of the

satellite dataset<sup>46</sup>. A detailed description of the procedure, the data, and also links to the final dataset can be found in Pekel et al.<sup>44</sup>, and Mentaschi et al.<sup>7</sup>.

For the purpose of determining AC in the present study, we consider shoreline dynamics data for a 32-year period (1984-2015) from Mentaschi et al.<sup>7</sup>. We assume that this time series is representative for present-day ambient shoreline changes and extrapolate the trend into the future using a probabilistic approach. For each location, we consider the time series of all transects that are within 5 km distance along the same coastline stretch. This acts as a spatial smoothing in order to filter out local trends and reflects changes at km scale, which are more relevant in a global scale analysis. It further ensures that each transect has sufficient data and compensates for gaps in the satellite measurements due to poor quality or lack of data. The original dataset comes with confidence indicators and low-confidence measurements are excluded from the analysis. Similarly, shoreline changes that exceed 5 km in a year are also excluded as outliers.

The above analysis results in sets of annual shoreline displacements for each point, which are sampled randomly to generate synthetic series of future shoreline position with an annual time step. The Monte Carlo sampling results in one million realizations of future shoreline evolution, resulting in Probability Density Functions (PDFs) of annual shoreline displacement during the present century in each transect. The number of realizations was taken to ensure a stable PDF of the shoreline changes by the end the century in all studied transects, i.e. when the mean and the standard deviation of the PDFs converged. The realizations of future shoreline evolution assume that ambient change will follow historical trends and express the uncertainty of the historical observations.

### 1.3 Shoreline retreat due to SLR

The estimation of the equilibrium shoreline retreat  $R$  of sandy coasts due to SLR is based on the Bruun rule<sup>18</sup>. This approach builds on the concept that the beach morphology tends to adapt to the prevailing wave climate and is given by:

$$R = \frac{1}{\tan\beta} SLR \quad 3$$

where  $\tan\beta$  is the active profile slope.

Projections of regional SLR up to the end of this century are available from a probabilistic, process-based approach<sup>47</sup> that combines the major factors contributing to SLR: impact of self-attraction and loading of

the ocean upon itself due to the long term alteration of ocean density changes, globally averaged steric sea-level change, dynamic sea-level change, surface mass balance of ice from glaciers and ice-caps, surface mass balance and ice dynamics of Greenland and Antarctic ice sheet, land-water storage and Glacial Isostatic Adjustment. Local smaller scale vertical land movements such as land subsidence due to for example ground water pumping are not included in the SLR projections.

The  $\tan\beta$  term in equation 3 expresses the slope of the active beach profile, which to date typically has been assumed to be constant (in space) in large scale studies<sup>9</sup>. Here, we use a newly released global dataset of active beach slopes<sup>23</sup>. The dataset has been created combining the MERIT digital elevation dataset<sup>48</sup> with the GEBCO bathymetry<sup>49</sup>. Beach profiles are generated along each sandy beach transect by combining the above bathymetric and topographic data. The offshore boundary of the active profile is defined by the furthest location from the coast with a depth equal to the depth of closure  $d_c$ . The latter is calculated using an adaptation of the original Hallermeier 1978<sup>50</sup> formula by Nicholls et al. 1998<sup>51</sup> for applications on longer time scales, given by:

$$d_c = 2.28H_{e,t} - 68.5 \left( \frac{H_{e,t}^2}{gT_{e,t}^2} \right) \quad 4$$

where  $H_{e,t}$  is the significant wave height that is exceeded only 12 hours per  $t$  years,  $T_{e,t}$  is the associated wave period, and  $g$  is the gravitational acceleration. In this case  $t$  is equivalent to the 1980-2100 period.

The landward active profile boundary varies among studies and has been defined as the crest of the berm or dune, or the most offshore location with an elevation equal to the MSL. In the absence of reliable estimates of the dune or berm height  $B$ , and following the original definition of the Bruun Rule<sup>18</sup> and its application in several recent studies<sup>9,52,53</sup>, here we take the MSL contour as the landward active profile boundary. The cross-shore distance between these two points is considered as the length of the active profile  $L_b$ , of which the slope is defined as  $\tan\beta = \frac{d_c}{L_b}$ .

Waves are simulated over the period 1980 to 2100 using the third generation spectral wave model WAVEWATCH-III forced by atmospheric conditions from 6 CMIP5 GCMs<sup>28,54</sup>. The model runs on a global  $1.5^\circ$  grid, combined with several nested finer sub-grids with resolution varying from  $0.5^\circ$  to  $0.5^\circ$ . The model's skill to reproduce global wave fields was assessed by comparing time series from a reanalysis covering 35 years between 1980 and 2014, forced by ERA-Interim wind data, against altimeter data provided by 6 different satellites<sup>55</sup>: ERS-2, ENVISAT, Jason 1 and 2, Cryosat 2 and SARAL-Altika. Point measurements provided by buoys were used for additional validation. Detailed information on the model set-up and validation can be found in the references provided<sup>28,54</sup>.

Several recent studies in Australia<sup>41</sup>, Netherlands<sup>56</sup>, Spain<sup>57</sup> and France<sup>58</sup> that compared coastline retreat projections obtained via the physics based Probabilistic coastline recession (PCR) model with those derived with the Bruun rule have indicated that the latter consistently provides higher-end estimates of coastline retreat. Acknowledging that the extent of overestimation depends on site-specific factors, we therefore include in our probabilistic framework a correction factor  $E$ , which varies randomly between 0.1 and 1.0 centered around a conservative median value 0.75. Thus, here we compute SLR driven shoreline retreat using the equation:

$$R = E \cdot \frac{1}{\tan\beta} \cdot SLR \quad 5$$

Finally, the active beach slope analysis detected that  $\tan\beta$  values in some parts of the world can be as mild as 1/800. According to the Bruun rule and the projected range of SLR, such mild sloping coastal zones will experience shoreline retreats of several hundreds of meters. While not impossible, such estimates could yield serious potential overestimations of real-world shoreline adjustment to SLR<sup>59</sup>. We therefore limit the minimum beach slope to 1/300, which is a realistic lower bound estimate for sandy beaches.

As SLR retreat is estimated in a probabilistic manner through Monte Carlo simulations, the resulting PDFs express the uncertainty from the SLR projections and the Bruun rule error expressed through the  $E$  correction factor.

#### 1.4 Storm-induced erosion

Episodic erosion during extreme storms is estimated using the convolution erosion model KD93 of Kriebel and Dean<sup>24</sup>. KD93 is based on the equilibrium profile concept and estimates shoreline retreat and volumetric sand loss due to extreme waves and storm surge. KD93 input can be classified in (i) hydrodynamic variables: significant wave height ( $H_s$ ), peak wave period ( $T_p$ ), wave incidence angle ( $\alpha_w$ ), storm surge ( $\eta_s$ ), tidal level ( $\eta_{tide}$ ) and event duration; and (ii) parameters related to the beach profile: dune height  $D$ , berm height  $B$  and width  $W$ , and the beach-face slope  $\tan\beta_f$ .

Storm surges for the present and future climate conditions are simulated using the DFLOW FM model<sup>60,61</sup> forced with the same 6-member CMIP5 Global Climate Model (GCM) ensemble as the wave projections<sup>20</sup> (described in the previous section).

The hydrodynamic conditions driving episodic beach erosion are obtained from the wave and storm surge projections. For each of the 6 GCMs we extracted the storm events simulated during the period

1980-2100, considering the parameters:  $\max H_s$ ,  $\eta_s$ ,  $\eta_{tide}$  and  $T_p$ , as well as mean wave direction  $Dir_w$ , and event duration. The extraction of storm events is based on the following criteria: (i) maximum  $H_s$  or  $\eta_s$  exceeding the 90<sup>th</sup> percentile value; (ii) maximum  $T_p$  above 3 s; and (iii) maximum  $H_s$  above 0.5 m.

The offshore wave conditions are transformed to the nearshore (50 m depth) through wave refraction, shoaling and breaking calculations based on Snell's law, following the approach described in Part II, Chapter 2 of the US Army Corps Coastal engineering Manual<sup>62</sup>. The wave incidence angle required for the calculations is obtained by combining the wave direction of each event from the model output with the mean shoreline orientation. The active beach slope is obtained from the global dataset mentioned above<sup>23</sup>.

Subsequently, we simulate storm induced erosion for all the above events using KD93 on equilibrium profiles, obtaining a sequence of shoreline retreat events for each transect. Subsequently, we apply non-stationary extreme value statistical analysis<sup>63</sup> and fit a generalized Pareto distribution to the retreat event series in order to obtain shoreline retreat estimates for different return periods. The present analysis focuses on the storm-induced shoreline retreat for the 100-year retreat event  $S_{100}$ , and its difference ( $\Delta S_{100}$ ) compared to present day conditions.

As storm retreat is estimated in a probabilistic manner through Monte Carlo simulations, the resulting PDFs express the uncertainty from the wave projections (i.e. GCM ensemble spread and ocean model error).

## 1.5 Spatial analysis

The study focusses on sandy beaches along the global coastline, which have been detected in a recent study by discretizing the coast at 500 m alongshore transects<sup>1</sup>. We use the Global Human Settlement Layer<sup>64</sup> to estimate the population in low-lying coastal areas (i.e. elevation <10 m MSL) within a distance of 25 km from each sandy beach transect. This serves as a proxy for the number of people benefiting from nearby sandy beaches; either receiving natural protection from coastal storms, or benefiting from beach amenity value, or other socio-economic activities related to tourism, beach-use, etc.

In order to identify regional patterns in shoreline dynamics, the global coastline is divided in 26 geographical regions (Extended Data Fig. 1), as defined in the IPCC Special Report on Managing the Risks of Extreme Events and Disasters to Advance Climate Change Adaptation<sup>65</sup>. The values discussed in the manuscript correspond to averages for each region and country, or for the entire global coastline.

## 1.6 Statistical analysis

Equations 1 and 2 are applied here in a probabilistic manner, with the assumption that shoreline change components  $R$ ,  $S$  and  $AC$  are independent. PDFs of the three components are combined through Monte Carlo simulations following the steps below<sup>20</sup>: (i) random sampling from the individual PDFs; (ii) linear addition of the  $dx_{shore}$  components according to equations 1 and 2; (iii) control of convergence to ensure that the number of realizations is sufficient; (iv) joint PDF estimation. Typically one million realizations are sufficient to obtain stable PDFs and convergence of the final percentiles. The resulting PDF of  $dx_{shore}$  expresses the joint contributions from all components and the uncertainty therein (uncertainty factors considered for each component are discussed in the final paragraph of the different dedicated sections 1.2-1.4).

We express the relative contribution of a component by the fraction of its median value to the median total retreat. Similarly, relative contributions to the total  $dx_{shore}$  uncertainty is expressed by the fraction of each component's variance to the total variance. We also estimate the difference between the median  $dx_{shore}$  values for RCP4.5 and RCP8.5.

## 1.7 Limitations

The spatial and temporal scale of the analysis presented here imposes inevitable limitations related to computational resources, data availability and methodological abstraction, the most important of which are discussed below.

Ambient shoreline trends can be an important component of shoreline dynamics and depend on several factors including the various sediment sources and sinks<sup>57</sup>, along with the fate of sediments<sup>66-68</sup>. While smaller-scale assessments considered in detail the above factors<sup>69</sup>, limitations in terms of modelling capabilities and available datasets, render application of such a methodology at global scale as impossible. Therefore, in the present analysis we extrapolate historically observed ambient shoreline changes  $AC$  into the future, as is common in previous studies<sup>58,70,71</sup>. This is done, however, in a probabilistic way that allows quantifying the temporal variability and inherent uncertainty. As such, future ambient shoreline dynamics follow ongoing trends within uncertainty bounds defined by the spread of the observed historical changes. The 32 year time window considered may be long enough to express decadal-scale variability in shoreline position, but still may not fully resolve some rare cases of coastline change, like those induced by very extreme events, or sudden and drastic human

interventions. Finally, the 30 m spatial resolution of the satellite dataset may not suffice to resolve smaller displacements in less energetic areas.

Shoreline retreat due to SLR is estimated using the Bruun rule<sup>18</sup>, which despite its known drawbacks is expected to be adequate for large scale assessments<sup>9,72</sup>. The Bruun rule is based on the concept that the morphology tends to reach an equilibrium state, which is supported by field observations<sup>40,73,74</sup>. However, the parameterization of the equilibrium profile *per se* has been a subject of debate<sup>75-77</sup>, as the simplified model excludes several factors controlling coastal morphology often found in nature. These include, for example, sediment sinks and sources<sup>69</sup>, morphological response to SLR<sup>59</sup>, morphological control from natural or artificial structures<sup>6</sup>, the presence of nearshore bars<sup>78</sup> or other morphological features<sup>79,80</sup> and longshore processes<sup>66</sup>.

Still, despite the criticism<sup>75</sup>, the concept is being used extensively because any proposed improvements and modifications<sup>53,81-85</sup> demand data that are often not available. In the present implementation several of the shortcomings of the Bruun rule are bypassed since  $R$  focusses only on what the concept can deliver; i.e. alongshore-averaged shoreline response to SLR and changes in wave climate. Most of the factors discussed above and that are beyond the Bruun rule's capacity are expressed by the ambient change AC: e.g. changes due to sediment budget imbalances, geological or anthropogenic factors.

The uncertainty related to the active profile slope is another common weakness of the Bruun rule<sup>41</sup>, which in the present analysis is addressed through the use of estimates obtained from topo-bathymetric data. The quantitative accuracy of Bruun rule estimates has also been the subject of rigorous debate for over 3 decades<sup>41,72,75,86</sup>. Here we have attempted to address this source of uncertainty by incorporating a correction factor  $E$  (Eq 5; see also discussion in Section 1.3), which is implemented probabilistically within the Monte Carlo framework adopted in our computations.

Beach profile responses to storms are simulated using the KD93 model, rather than with sophisticated process-based models that incorporate elaborate numerical methods and sediment transport modules<sup>87-93</sup>. Such models can potentially provide more accurate estimations of storm erosion (if they are well calibrated and validated), but require as input detailed topo-bathymetric and sediment grain size information that is not available at global scale. The present analysis of  $S$  required the simulation of circa 45 million storm events, rendering the application of models that are computationally more expensive than KD93 practically impossible. In addition, KD93 has produced acceptable results in previous smaller-scale applications of similar scope<sup>94-96</sup>.

An aspect not covered in our analysis is the effect of storm clusters. It has been discussed extensively in previous studies, based either on field data<sup>40,42</sup>, or numerical models<sup>87,97-99</sup>, that storm chronology can enhance the impact of individual events. These studies have also shown that storm erosion can be followed by beach recovery. The latter is a complex process that is difficult to simulate<sup>73,100</sup> and requires in situ data. Predicting the maximum erosion from storm clusters at global scale is therefore a challenging task. We consider only the episodic erosion from individual storms without accounting for storm groups and do not simulate post-storm recovery. Rather it is assumed that the combined, long-term, residual effects of erosion and recovery are included in the ambient change component AC.

The present analysis assumes unlimited backshore space for shoreline retreat. Some natural coastal systems may have such accommodation space, while in other sites this may be strongly limited by human development or physical barriers. This is a known issue which combined with SLR can have societal and ecological implications discussed in the literature, especially under the term of coastal squeeze<sup>101,102</sup>. In principle, satellite imagery could provide information on beach width<sup>103</sup> and available space for coastal retreat at the backshore, yet such global dataset is not available. Socio-economic projections suggest that coastal development will most likely continue in the decades to come<sup>12,13</sup>, which may further reduce the accommodating space for coastal retreat. We consider arbitrary erosion threshold values to indicate potential changes that could be critical for sandy beaches. With the information on backshore space and development that may be available at local/regional scales, our publicly available projections could be used by scientists and practitioners to carry out more detailed smaller-scale assessments.

## 1.8 Additional Results

### Sea level rise retreat

Rising sea levels will result in shoreline retreat along the entire global coastline with the exception of a few regions that experience uplift, like the Baltic Sea (Extended Data Fig. 2). The global average median  $R$  by 2050 (relative to 2010) is projected to be around -28 m and -35 m under RCP4.5 and RCP8.5, respectively. By the end of the century, SLR-driven erosion is projected to further grow to around -63 m and -105 m, respectively. The retreat of sandy beaches due to SLR is projected to be highest (at least 130 m by 2100 relative to 2010 under RCP8.5) in North Australia, Central North America, North-East Brazil, South and Southeast Asia, and Central Europe. Other regions for which high  $R$  values are projected include West Africa, Southeastern South America, South Australia/New Zealand, East Asia and East North America.



## Ambient changes

The present section discusses long-term ambient changes as a result of hydrodynamic, geological and anthropic factors. The global averaged AC is erosive, corresponding to global average land retreat of -11.5 m by 2050 (very likely range between -34.7 and 11.7 m) and of -30.4 m by the end of the century (very likely range between -79.1 and 18.2 m). The stronger erosion is projected for South Asia, the Caribbean SIDS, and Southeastern South America with the very likely range by the end of the century being from -431.8 to -238.2, from -250 to -174.2, and from -204.5 to -71.3, respectively (Extended Data Fig. 3). East Asia shows a strong accretive ambient shoreline change trend (very likely range: 86.7-147.6), being the result of major coastal land reclamations over the recent decades.

Smaller scale projections show high spatial variability with erosive and accretive trends interchanging. Examples of accretion hotspots in Central America/Mexico can be found in Colombia, both on the Caribbean Sea and on the Pacific Ocean, especially at the mouths of the rivers Atrato, Sinu, Magdalena, Jurubida, San Juan and others. In Central North America, the long-term trends of coastal erosion/accretion are dominated by the dynamics at the mouth of the Mississippi river. The area is very dynamic, with large erosive spots (e.g. the Terrebonne Bay) and accretive spots (e.g. the Atchafalaya delta<sup>104</sup>). Furthermore, the area is frequently hit by tropical cyclones<sup>105</sup> that may cause abrupt extreme erosion, for example hurricane Katrina, the largest natural disaster in the history of the US<sup>106</sup>, and hurricane Rita in 2005.

In North-Eastern Brazil, the activity is dominated by the morpho-dynamics of the Tocantins delta and along the coasts of Para-Maranhao-Piaui-Ceara, a very active area characterized by both extreme coastal erosion and accretion<sup>7</sup>. The dominance of accretion is likely due to the erosivity of the soil in the interior, a rich river network that transports sediments towards the sea, and strong macro-tidal currents carrying them along the coasts<sup>107</sup>.

The most active areas in Southern Africa are the coasts of Mozambique and the Western coasts of Madagascar, areas characterized by intense tidal currents. Accretion prevails especially in Madagascar, likely due to internal erosion and subsequent transport of sediment towards the coasts, and redistribution of it by currents<sup>108</sup>.

Southeast Asia is characterized by both extreme erosion and accretion. Intense erosion can be observed, for example, at the deltas of the rivers Sittaung<sup>109</sup> and Mekong<sup>19</sup>, or in areas of strong land subsidence, like the Northern coast of Java<sup>110</sup>, or in the northern Manila Bay<sup>111</sup>. Examples of areas dominated by extreme accretion are the extended delta of the Red river in North Vietnam, western New Guinea,

several river deltas in the Malaysian peninsula and Sumatra, as well as in intensely built sites such as Bangkok and Singapore. A more detailed discussion on the local/regional variations can be found in Mentaschi et al.<sup>7</sup>.

## Acknowledgments

RR is supported by the AXA Research fund and the Deltares Strategic Research Programme 'Coastal and Offshore Engineering'. PA is supported by the EU Horizon 2020 Programme for Research and Innovation, under grant agreement no. 776613 (EUCP: European Climate Prediction system).

## Author contributions

M.I.V, R.R. and L.F. jointly conceived the study. M.I.V. and L.M. produced the storm surge and wave projections. L.M. produced the ambient shoreline change data. M.I.V. and T.A.P. produced the storm erosion and sea level rise retreat projections, P.A. produced the global beach slope dataset, A.L. produced the global sandy beach presence dataset. M.I.V. analysed the data and prepared the manuscript, with all authors discussing results and implications and commenting on the manuscript at all stages. T.P. was funded by the research group RNM-328 of the Andalusian Research Plan (PAI) and the Portuguese Science and Technology Foundation (FCT) through the grant UID/MAR/00350/2013 attributed to CIMA of the University of Algarve. The corresponding author would like to thank Drs Alessio Giardino and Ap van Dongeren for providing helpful comments on the manuscript and the methodology.

**Competing interests:** the Authors declare no Competing Financial or Non-Financial Interest

## Data availability

The models and datasets presented are part of the integrated risk assessment tool LISCoAsT (Large scale Integrated Sea-level and Coastal Assessment Tool) developed by the Joint Research Centre of the European Commission. The dataset is available through the LISCoAsT repository of the JRC data collection (<http://data.europa.eu/89h/18eb5f19-b916-454f-b2f5-88881931587e>) and should be cited as follows:

European Commission, Joint Research Centre (2019): Global shoreline change projections.

European Commission, Joint Research Centre (JRC) [Dataset] doi:10.2905/18EB5F19-B916-454F-B2F5-88881931587E; PID: <http://data.europa.eu/89h/18eb5f19-b916-454f-b2f5-88881931587e>

## Code availability

The code that supported the findings of this study is available from the corresponding author upon reasonable request.

## Methods References

- 33 Meinshausen, M. *et al.* The RCP greenhouse gas concentrations and their extensions from 1765 to 2300. *Clim. Change* **109**, 213-241, doi:10.1007/s10584-011-0156-z (2011).
- 34 Hurst, M. D., Rood, D. H., Ellis, M. A., Anderson, R. S. & Dornbusch, U. Recent acceleration in coastal cliff retreat rates on the south coast of Great Britain. *Proceedings of the National Academy of Sciences* **113**, 13336-13341, doi:10.1073/pnas.1613044113 (2016).
- 35 Ruggiero, P. Is the Intensifying Wave Climate of the U.S. Pacific Northwest Increasing Flooding and Erosion Risk Faster Than Sea-Level Rise? *Journal of Waterway, Port, Coastal, and Ocean Engineering* **139**, 88-97, doi:doi:10.1061/(ASCE)WW.1943-5460.0000172 (2013).
- 36 Loureiro, C., Ferreira, Ó. & Cooper, J. A. G. Extreme erosion on high-energy embayed beaches: Influence of megarips and storm grouping. *Geomorphology* **139–140**, 155-171, doi:http://dx.doi.org/10.1016/j.geomorph.2011.10.013 (2012).
- 37 Kroon, A. *et al.* Statistical analysis of coastal morphological data sets over seasonal to decadal time scales. *Coastal Eng.* **55**, 581-600 (2008).
- 38 Gallop, S. L., Bosserelle, C., Pattiaratchi, C. & Eliot, I. Rock topography causes spatial variation in the wave, current and beach response to sea breeze activity. *Mar. Geol.* **290**, 29-40, doi:10.1016/j.margeo.2011.10.002 (2011).
- 39 Voudoukas, M. I., Velegrakis, A. F. & Plomaritis, T. A. Beachrock occurrence, characteristics, formation mechanisms and impacts. *Earth-Science Reviews* **85**, 23-46, doi:10.1016/j.earscirev.2007.07.002 (2007).
- 40 Voudoukas, M. I., Almeida, L. P. & Ferreira, Ó. Beach erosion and recovery during consecutive storms at a steep-sloping, meso-tidal beach. *Earth Surf. Processes Landforms* **37**, 583-691, doi:10.1002/esp.2264 (2012).
- 41 Ranasinghe, R., Callaghan, D. & Stive, M. J. F. Estimating coastal recession due to sea level rise: beyond the Bruun rule. *Clim. Change* **110**, 561-574, doi:10.1007/s10584-011-0107-8 (2012).
- 42 Coco, G. *et al.* Beach response to a sequence of extreme storms. *Geomorphology* **204**, 493-501, doi:http://dx.doi.org/10.1016/j.geomorph.2013.08.028 (2014).
- 43 Hardisty, J. in *Sediment Transport and Depositional Processes* (ed K. Pye) 216-255 (Blackwell, 1994).
- 44 Pekel, J.-F., Cottam, A., Gorelick, N. & Belward, A. S. High-resolution mapping of global surface water and its long-term changes. *Nature* **540**, 418, doi:10.1038/nature20584  
<https://www.nature.com/articles/nature20584#supplementary-information> (2016).
- 45 Haklay, M. & Weber, P. OpenStreetMap: User-Generated Street Maps. *IEEE Pervasive Computing* **7**, 12-18, doi:10.1109/MPRV.2008.80 (2008).
- 46 Boak, E. H. & Turner, I. L. Shoreline Definition and Detection: A Review. *J. Coast. Res.*, 688-703, doi:doi:10.2112/03-0071.1 (2005).
- 47 Jackson, L. P. & Jevrejeva, S. A probabilistic approach to 21st century regional sea-level projections using RCP and High-end scenarios. *Global Planet. Change* **146**, 179-189, doi:http://dx.doi.org/10.1016/j.gloplacha.2016.10.006 (2016).
- 48 Yamazaki, D. *et al.* A high-accuracy map of global terrain elevations. *Geophys. Res. Lett.* **44**, 5844-5853, doi:doi:10.1002/2017GL072874 (2017).

624 49 Weatherall, P. *et al.* A new digital bathymetric model of the world's oceans. *Earth and Space*  
 625 *Science* **2**, 331-345, doi:doi:10.1002/2015EA000107 (2015).  
 626 50 Hallermeier, R. J. in *16th International Conference on Coastal Engineering*.1493-1512 (ASCE).  
 627 51 Nicholls, R. J., Birkemeier, W. A. & Lee, G.-h. Evaluation of depth of closure using data from  
 628 Duck, NC, USA. *Mar. Geol.* **148**, 179-201 (1998).  
 629 52 Baron, H. M. *et al.* Incorporating climate change and morphological uncertainty into coastal  
 630 change hazard assessments. *Nat. Hazards* **75**, 2081-2102, doi:10.1007/s11069-014-1417-8  
 631 (2015).  
 632 53 Ranasinghe, R., Duong, T. M., Uhlenbrook, S., Roelvink, D. & Stive, M. Climate-change impact  
 633 assessment for inlet-interrupted coastlines. *Nature Climate Change* **3**, 83,  
 634 doi:10.1038/nclimate1664  
 635 <https://www.nature.com/articles/nclimate1664#supplementary-information> (2012).  
 636 54 Vousdoukas, M. I., Mentaschi, L., Voukouvalas, E., Verlaan, M. & Feyen, L. Extreme sea levels on  
 637 the rise along Europe's coasts. *Earth's Future*, n/a-n/a, doi:10.1002/2016EF000505 (2017).  
 638 55 Queffelec, P. & Croizé-Fillon, D. Global altimeter SWH data set. (Laboratoire d'Océanographie  
 639 Spatiale, IFREMER, 2014).  
 640 56 Li, F. *Probabilistic estimation of dune erosion and coastal zone risk* PhD Thesis thesis, Delft  
 641 University of Technology, (2014).  
 642 57 Toimil, A., Losada, I. J., Camus, P. & Díaz-Simal, P. Managing coastal erosion under climate  
 643 change at the regional scale. *Coastal Eng.* **128**, 106-122,  
 644 doi:https://doi.org/10.1016/j.coastaleng.2017.08.004 (2017).  
 645 58 Le Cozannet, G. *et al.* Quantifying uncertainties of sandy shoreline change projections as sea  
 646 level rises. *Scientific Reports* **9**, 42, doi:10.1038/s41598-018-37017-4 (2019).  
 647 59 Lentz, E. E. *et al.* Evaluation of dynamic coastal response to sea-level rise modifies inundation  
 648 likelihood. *Nature Clim. Change* **6**, 696–700, doi:10.1038/nclimate2957  
 649 [http://www.nature.com/nclimate/journal/vaop/ncurrent/abs/nclimate2957.html#supplementary-](http://www.nature.com/nclimate/journal/vaop/ncurrent/abs/nclimate2957.html#supplementary-information)  
 650 [information](http://www.nature.com/nclimate/journal/vaop/ncurrent/abs/nclimate2957.html#supplementary-information) (2016).  
 651 60 Jagers, B. R., J. L.; Verlaan, M.; Lalic, A.; Genseberger, M.; Friocourt, Y.; van der Pijl, S. in  
 652 *American Geophysical Union, Fall Meeting 2014*(San Francisco, USA, 2014).  
 653 61 Muis, S., Verlaan, M., Winsemius, H. C., Aerts, J. C. J. H. & Ward, P. J. A global reanalysis of storm  
 654 surges and extreme sea levels. *Nat Commun* **7**, doi:10.1038/ncomms11969 (2016).  
 655 62 US Army Corps of Engineers. *Coastal Engineering Manual*.(U.S. Army Corps of Engineers, 2002).  
 656 63 Mentaschi, L. *et al.* Non-stationary Extreme Value Analysis: a simplified approach for Earth  
 657 science applications. *Hydrol. Earth Syst. Sci. Discuss.* **2016**, 1-38, doi:10.5194/hess-2016-65  
 658 (2016).  
 659 64 Corbane, C. *et al.* Big earth data analytics on Sentinel-1 and Landsat imagery in support to global  
 660 human settlements mapping. *Big Earth Data* **1**, 118-144, doi:10.1080/20964471.2017.1397899  
 661 (2017).  
 662 65 IPCC. *Managing the Risks of Extreme Events and Disasters to Advance Climate Change*  
 663 *Adaptation. A Special Report of Working Groups I and II of the Intergovernmental Panel on*  
 664 *Climate Change*.(Cambridge University Press, 2012).  
 665 66 Antolínez, J. A. A. *et al.* A multiscale climate emulator for long-term morphodynamics (MUSCLE-  
 666 morpho). *Journal of Geophysical Research: Oceans* **121**, 775-791, doi:doi:10.1002/2015JC011107  
 667 (2016).  
 668 67 Enríquez, A. R., Marcos, M., Álvarez-Ellacuría, A., Orfila, A. & Gomis, D. Changes in beach  
 669 shoreline due to sea level rise and waves under climate change scenarios: application to the

- Balearic Islands (western Mediterranean). *Nat. Hazards Earth Syst. Sci.* **17**, 1075-1089, doi:10.5194/nhess-17-1075-2017 (2017).
- 68 Anderson, D., Ruggiero, P., Antolínez, J. A. A., Méndez, F. J. & Allan, J. A Climate Index Optimized for Longshore Sediment Transport Reveals Interannual and Multidecadal Littoral Cell Rotations. *Journal of Geophysical Research: Earth Surface* **123**, 1958-1981, doi:10.1029/2018JF004689 (2018).
- 69 Giardino, A. *et al.* A quantitative assessment of human interventions and climate change on the West African sediment budget. *Ocean Coast. Manag.* **156**, 249-265, doi:https://doi.org/10.1016/j.ocecoaman.2017.11.008 (2018).
- 70 Vitousek, S., Barnard, P. L., Limber, P., Erikson, L. & Cole, B. A model integrating longshore and cross-shore processes for predicting long-term shoreline response to climate change. *Journal of Geophysical Research: Earth Surface* **122**, 782-806, doi:10.1002/2016jf004065 (2017).
- 71 Wainwright, D. J. *et al.* Moving from deterministic towards probabilistic coastal hazard and risk assessment: Development of a modelling framework and application to Narrabeen Beach, New South Wales, Australia. *Coastal Eng.* **96**, 92-99, doi:https://doi.org/10.1016/j.coastaleng.2014.11.009 (2015).
- 72 Ranasinghe, R. & Stive, M. J. F. Rising seas and retreating coastlines. *Clim. Change* **97**, 465, doi:10.1007/s10584-009-9593-3 (2009).
- 73 Davidson, M. A., Splinter, K. D. & Turner, I. L. A simple equilibrium model for predicting shoreline change. *Coastal Eng.* **73**, 191-202, doi:http://dx.doi.org/10.1016/j.coastaleng.2012.11.002 (2013).
- 74 Ozkan-Haller, T., Brundidge, S. Equilibrium Beach Profiles for Delaware Beaches. 147-160 (2007).
- 75 Cooper, J. A. G. & Pilkey, O. H. Sea-level rise and shoreline retreat: time to abandon the Bruun Rule. *Global Planet. Change* **43**, 157-171, doi:http://dx.doi.org/10.1016/j.gloplacha.2004.07.001 (2004).
- 76 Pilkey, O. H. & Dixon, K. L. *The Corps and the Shore*. (Island Press, 1996).
- 77 Pilkey, O. H. *et al.* The Concept of Shoreface Profile of Equilibrium: A Critical Review. *Journal of Coastal Research SI* **9**, 225-278 (1993).
- 78 Holman, R. A., Lalejini, D. M., Edwards, K. & Veeramony, J. A parametric model for barred equilibrium beach profiles. *Coastal Eng.* **90**, 85-94, doi:http://dx.doi.org/10.1016/j.coastaleng.2014.03.005 (2014).
- 79 Coco, G. & Murray, A. B. Patterns in the sand: From forcing templates to self-organization. *Geomorphology* **91**, 271-290, doi:10.1016/j.geomorph.2007.04.023 (2007).
- 80 Voudoukas, M. I. Erosion/accretion and multiple beach cusp systems on a meso-tidal, steeply-sloping beach. *Geomorphology* **141-142**, 34-46, doi:doi:10.1016/j.geomorph.2011.12.003 (2012).
- 81 Wang, Z. & Dean, R. G. in *Coastal Sediments '07* 626-632 (American Society of Civil Engineers, 2007).
- 82 Dai, Z.-J., Du, J.-z., Li, C.-C. & Chen, Z.-S. The configuration of equilibrium beach profile in South China. *Geomorphology* **86**, 441-454, doi:http://dx.doi.org/10.1016/j.geomorph.2006.09.016 (2007).
- 83 Romanczyk, W., Boczar-Karakiewicz, B. & Bona, J. L. Extended equilibrium beach profiles. *Coastal Eng.* **52**, 727-744, doi:https://doi.org/10.1016/j.coastaleng.2005.05.002 (2005).
- 84 Anderson, T. R., Fletcher, C. H., Barbee, M. M., Frazer, L. N. & Romine, B. M. Doubling of coastal erosion under rising sea level by mid-century in Hawaii. *Nat. Hazards* **78**, 75-103, doi:10.1007/s11069-015-1698-6 (2015).
- 85 Bray, M. & Hooke, J. Prediction of soft-cliff retreat with accelerating sea-level rise. *J. Coast. Res.* **13**, 453-467 (1997).

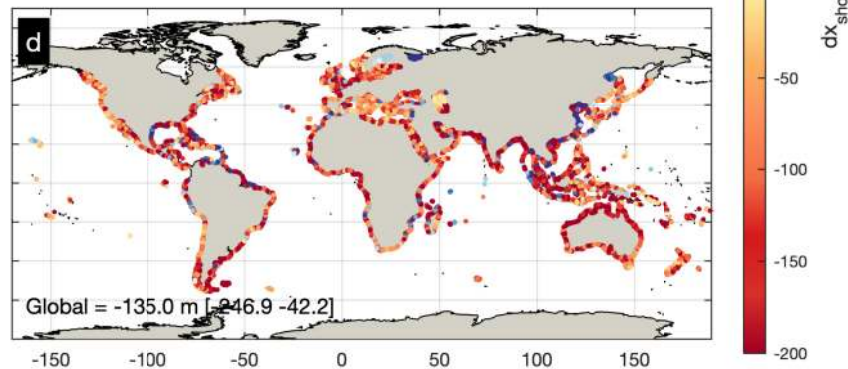
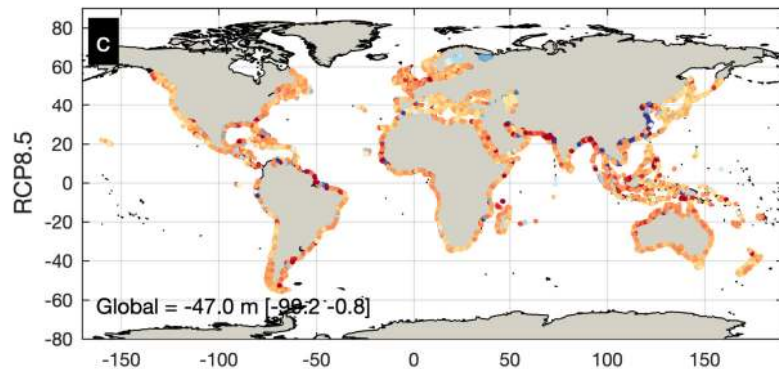
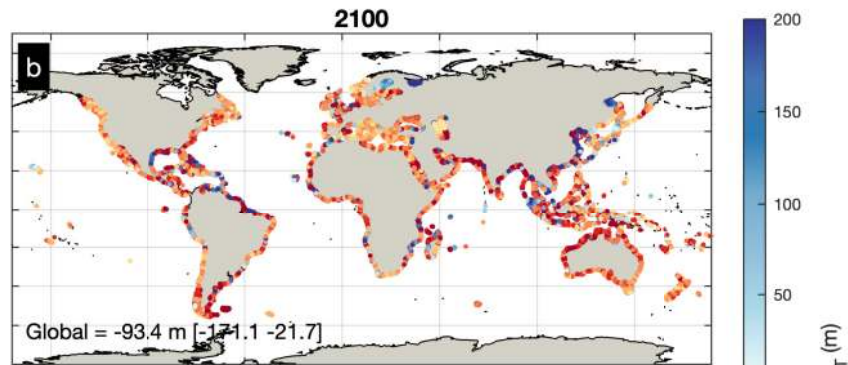
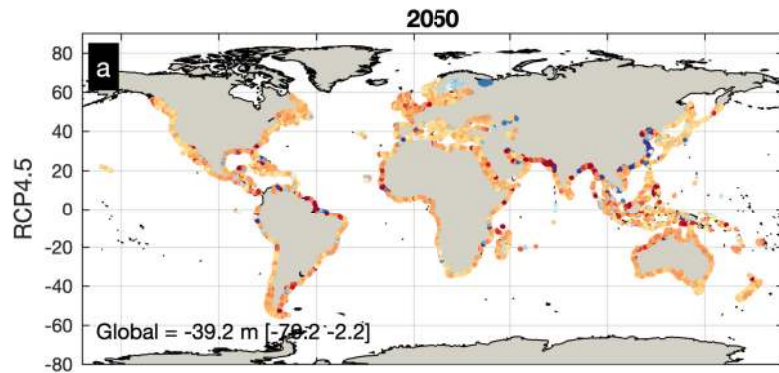
718 86 Pilkey, O. H. & Cooper, J. A. G. Society and Sea Level Rise. *Science* **303**, 1781,  
 719 doi:10.1126/science.1093515 (2004).  
 720 87 Splinter, K. D., Carley, J. T., Golshani, A. & Tomlinson, R. A relationship to describe the  
 721 cumulative impact of storm clusters on beach erosion. *Coastal Eng.* **83**, 49-55,  
 722 doi:http://dx.doi.org/10.1016/j.coastaleng.2013.10.001 (2014).  
 723 88 Vousdoukas, M. I., Ferreira, O., Almeida, L. P. & Pacheco, A. Toward reliable storm-hazard  
 724 forecasts: XBeach calibration and its potential application in an operational early-warning  
 725 system. *Ocean Dyn.* **62**, 1001-1015, doi:10.1007/s10236-012-0544-6 (2012).  
 726 89 Roelvink, D. *et al.* Modelling storm impacts on beaches, dunes and barrier islands. *Coastal Eng.*  
 727 **56**, 1133-1152 (2009).  
 728 90 Broekema, Y. B. *et al.* Observations and modelling of nearshore sediment sorting processes  
 729 along a barred beach profile. *Coastal Eng.* **118**, 50-62,  
 730 doi:https://doi.org/10.1016/j.coastaleng.2016.08.009 (2016).  
 731 91 de Winter, R. C. & Ruessink, B. G. Sensitivity analysis of climate change impacts on dune erosion:  
 732 case study for the Dutch Holland coast. *Clim. Change* **141**, 685-701, doi:10.1007/s10584-017-  
 733 1922-3 (2017).  
 734 92 Karunaratna, H., Brown, J., Chatzirodou, A., Dissanayake, P. & Wisse, P. Multi-timescale  
 735 morphological modelling of a dune-fronted sandy beach. *Coastal Eng.* **136**, 161-171,  
 736 doi:https://doi.org/10.1016/j.coastaleng.2018.03.005 (2018).  
 737 93 Passeri, D. L., Bilskie, M. V., Plant, N. G., Long, J. W. & Hagen, S. C. Dynamic modeling of barrier  
 738 island response to hurricane storm surge under future sea level rise. *Clim. Change* **149**, 413-425,  
 739 doi:10.1007/s10584-018-2245-8 (2018).  
 740 94 Callaghan, D. P., Nielsen, P., Short, A. D. & Ranasinghe, R. Statistical simulation of wave climate  
 741 and extreme beach erosion. *Coastal Eng.* **55**, 375-390 (2008).  
 742 95 Ferreira, Ó., Garcia, T., Matias, A., Taborda, R. & Dias, J. A. An integrated method for the  
 743 determination of set-back lines for coastal erosion hazards on sandy shores. *Cont. Shelf Res.* **26**,  
 744 1030-1044 (2006).  
 745 96 Mull, J. & Ruggiero, P. Estimating Storm-Induced Dune Erosion and Overtopping along U.S. West  
 746 Coast Beaches. *J. Coast. Res.*, 1173-1187, doi:10.2112/JCOASTRES-D-13-00178.1 (2014).  
 747 97 Ferreira, Ó. Storm groups versus extreme single storms: Predicted erosion and management  
 748 consequences. *Journal of Coastal Research* **42**, 155-161 (2005).  
 749 98 Dissanayake, P., Brown, J. & Karunaratna, H. Impacts of storm chronology on the  
 750 morphological changes of the Formby beach and dune system, UK. *Nat. Hazards Earth Syst. Sci.*  
 751 *Discuss.* **3**, 2565-2597, doi:10.5194/nhessd-3-2565-2015 (2015).  
 752 99 Hackney, C., Darby, S. E. & Leyland, J. Modelling the response of soft cliffs to climate change: A  
 753 statistical, process-response model using accumulated excess energy. *Geomorphology* **187**, 108-  
 754 121, doi:https://doi.org/10.1016/j.geomorph.2013.01.005 (2013).  
 755 100 Yates, M. L., Guza, R. T. & O'Reilly, W. C. Equilibrium shoreline response: Observations and  
 756 modeling. *Journal of Geophysical Research C: Oceans* **114** (2009).  
 757 101 Pontee, N. Defining coastal squeeze: A discussion. *Ocean Coast. Manag.* **84**, 204-207,  
 758 doi:https://doi.org/10.1016/j.ocecoaman.2013.07.010 (2013).  
 759 102 Doody, J. P. Coastal squeeze and managed realignment in southeast England, does it tell us  
 760 anything about the future? *Ocean Coast. Manag.* **79**, 34-41,  
 761 doi:https://doi.org/10.1016/j.ocecoaman.2012.05.008 (2013).  
 762 103 Monioudi, I. N. *et al.* Assessment of island beach erosion due to sea level rise: the case of the  
 763 Aegean archipelago (Eastern Mediterranean). *Nat. Hazards Earth Syst. Sci.* **17**, 449-466,  
 764 doi:10.5194/nhess-17-449-2017 (2017).

765 104 Rosen, T. & Xu, Y. J. Recent decadal growth of the Atchafalaya River Delta complex: Effects of  
 766 variable riverine sediment input and vegetation succession. *Geomorphology* **194**, 108-120,  
 767 doi:<https://doi.org/10.1016/j.geomorph.2013.04.020> (2013).  
 768 105 Peduzzi, P. *et al.* Global trends in tropical cyclone risk. *Nature Clim. Change* **2**, 289-294,  
 769 doi:[http://www.nature.com/nclimate/journal/v2/n4/abs/nclimate1410.html#supplementary-](http://www.nature.com/nclimate/journal/v2/n4/abs/nclimate1410.html#supplementary-information)  
 770 information (2012).  
 771 106 Travis, J. Scientists's Fears Come True as Hurricane Floods New Orleans. *Science* **309**, 1656,  
 772 doi:10.1126/science.309.5741.1656 (2005).  
 773 107 Monteiro, M. C., Pereira, L. C. C. & de Oliveira, S. M. O. Morphodynamic Changes of a Macrotidal  
 774 Sand Beach in the Brazilian Amazon Coast (Ajuruteua-Pará). *J. Coast. Res.*, 103-107 (2009).  
 775 108 Salomon, J.-N. L'accrétion littorale sur la côte Ouest de Madagascar. *Physio-Géo* **3**,  
 776 doi:10.4000/physio-geo.671 (2009).  
 777 109 Taft, L. & Evers, M. A review of current and possible future human–water dynamics in  
 778 Myanmar's river basins. *Hydrol. Earth Syst. Sci.* **20**, 4913-4928, doi:10.5194/hess-20-4913-2016  
 779 (2016).  
 780 110 Marfai, M. A. & King, L. Monitoring land subsidence in Semarang, Indonesia. *Environ. Geol.* **53**,  
 781 651-659, doi:10.1007/s00254-007-0680-3 (2007).  
 782 111 Rodolfo, K. S. & Siringan, F. P. Global sea-level rise is recognised, but flooding from  
 783 anthropogenic land subsidence is ignored around northern Manila Bay, Philippines. *Disasters* **30**,  
 784 118-139, doi:10.1111/j.1467-9523.2006.00310.x (2006).

785

786

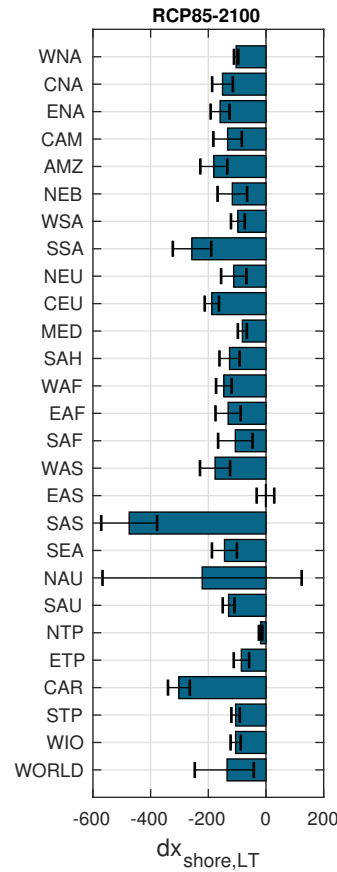
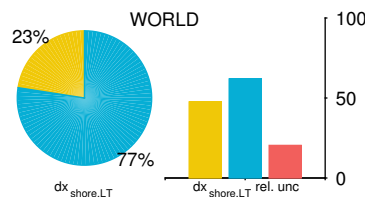
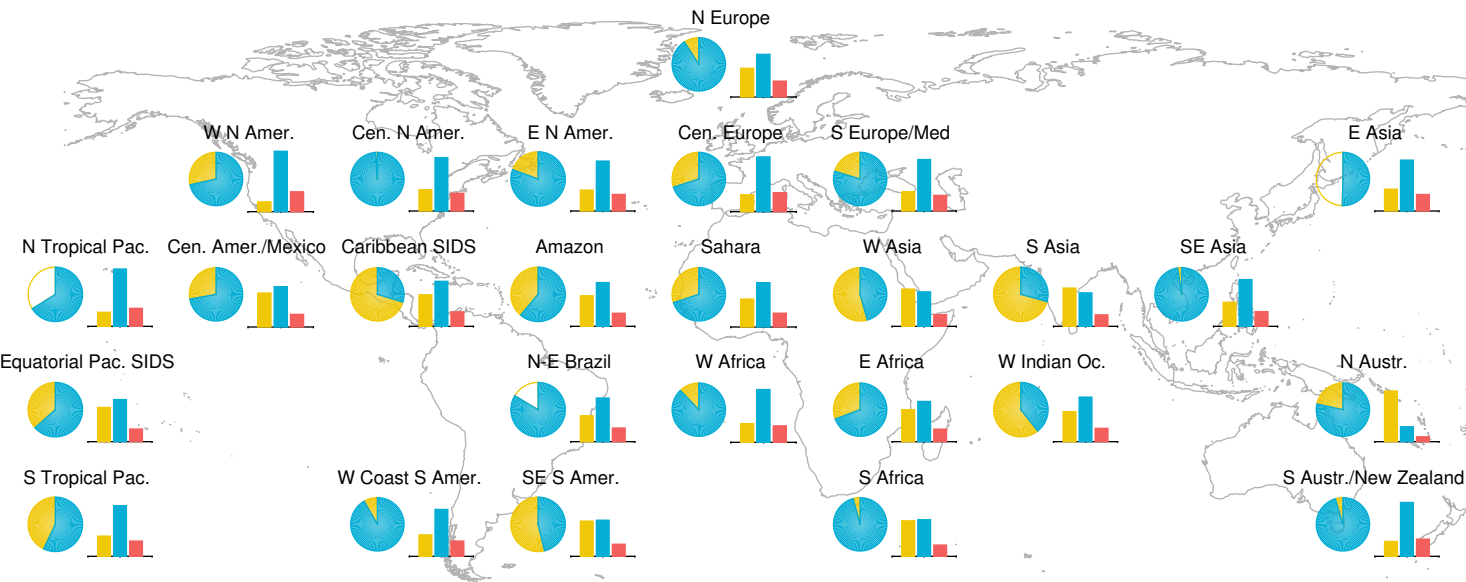
787

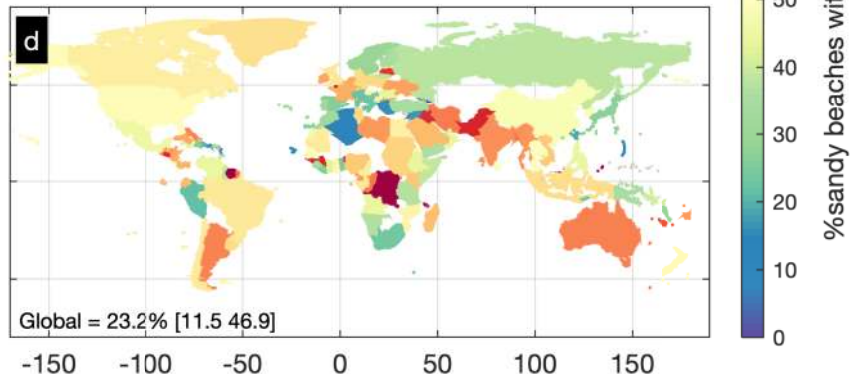
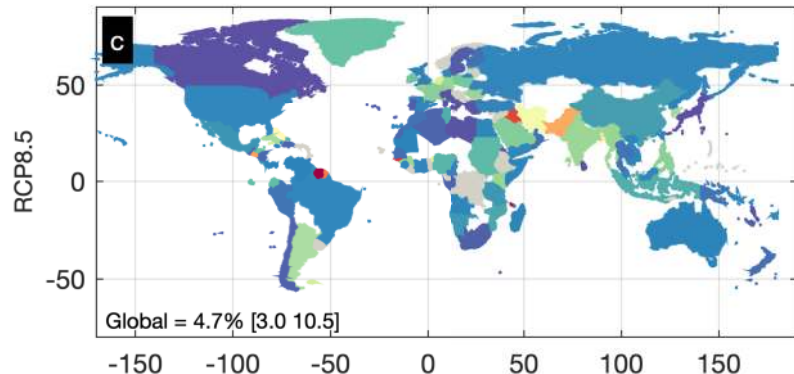
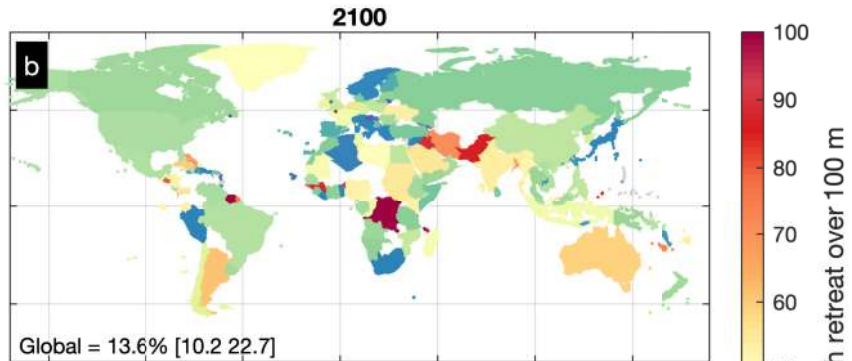
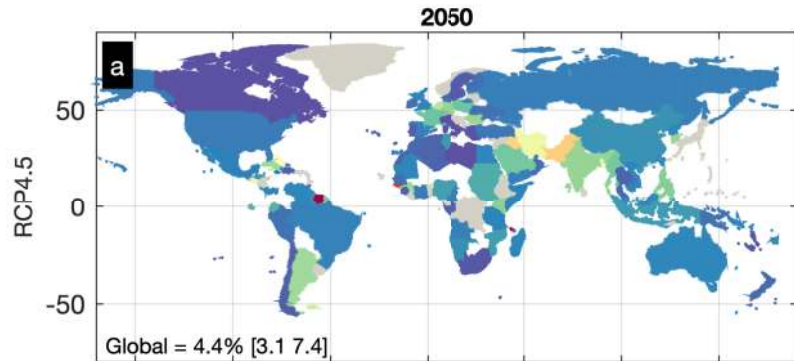


$dx_{shore,LT}$  (m)

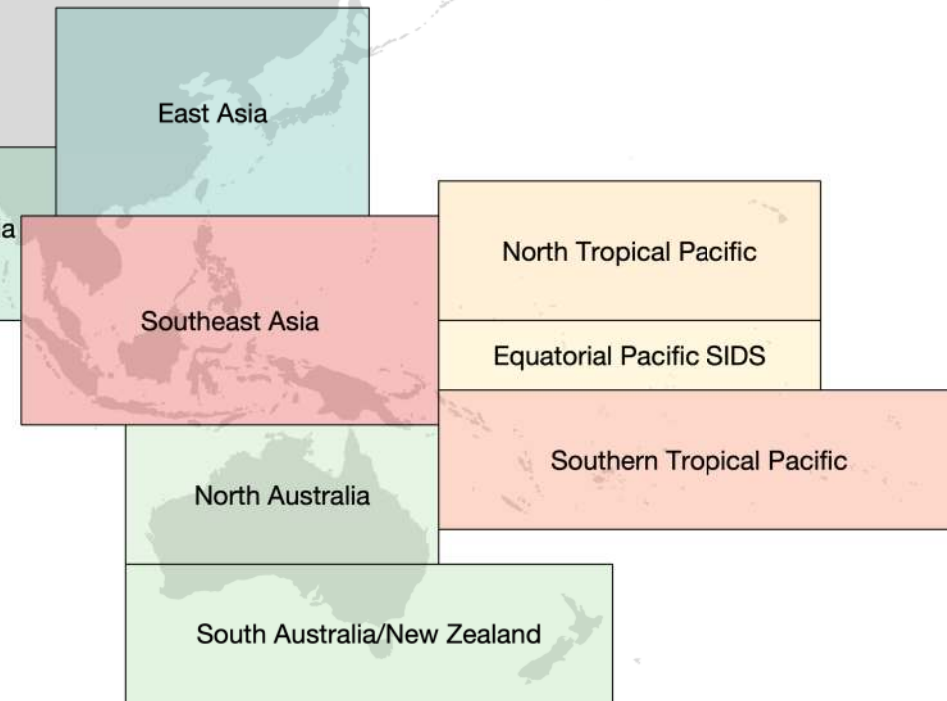
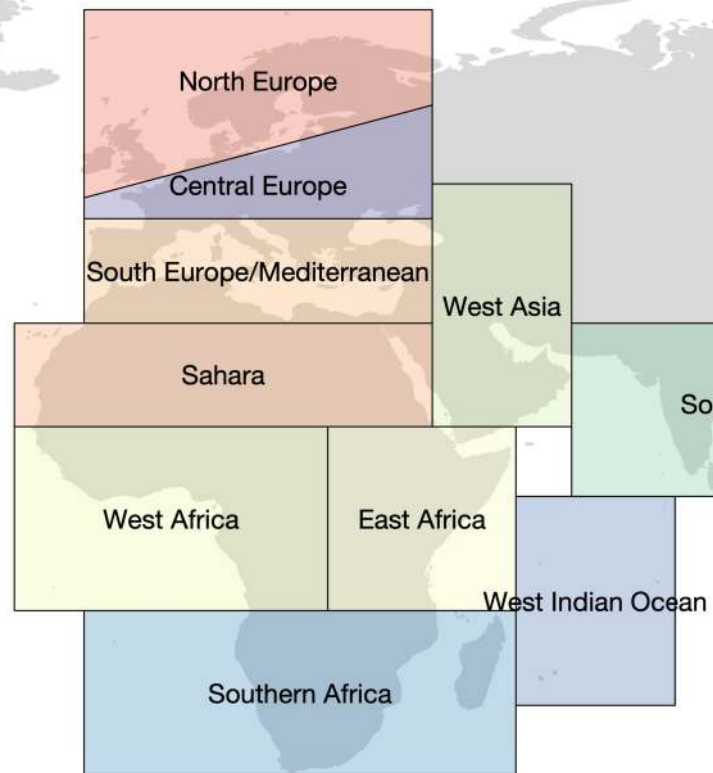
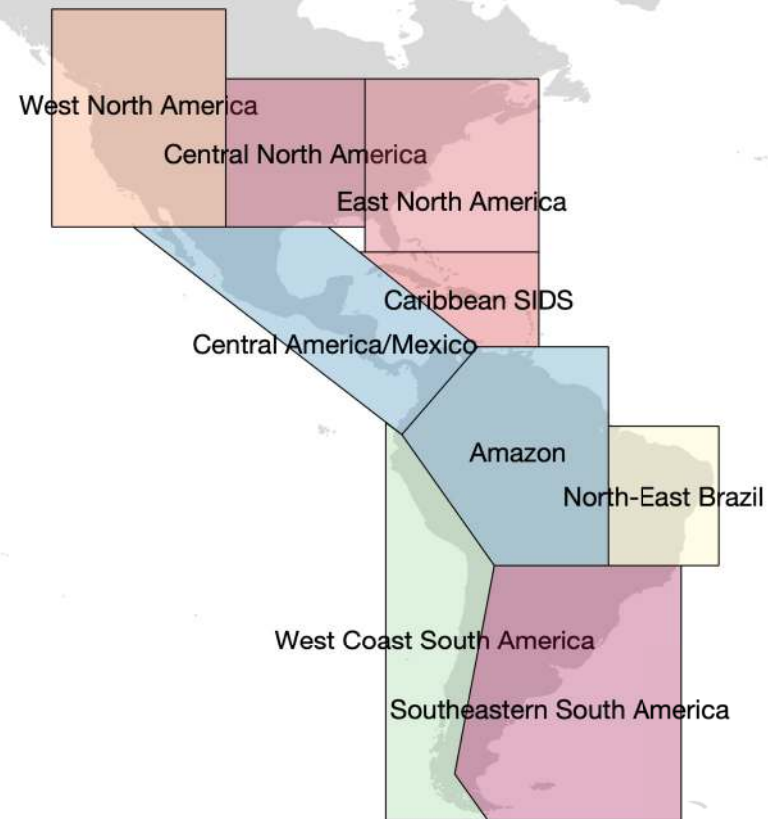


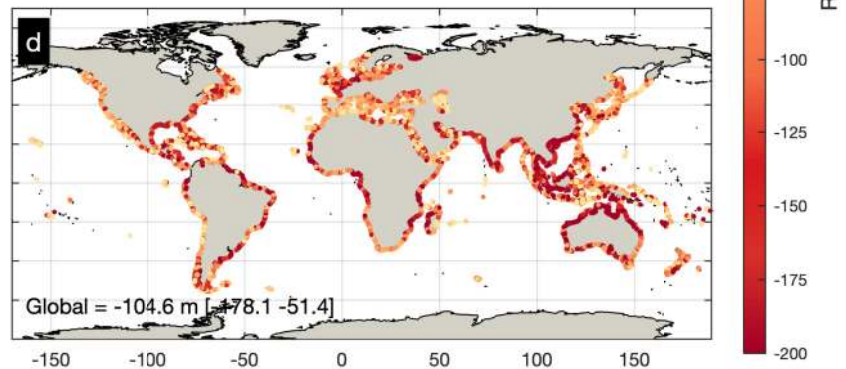
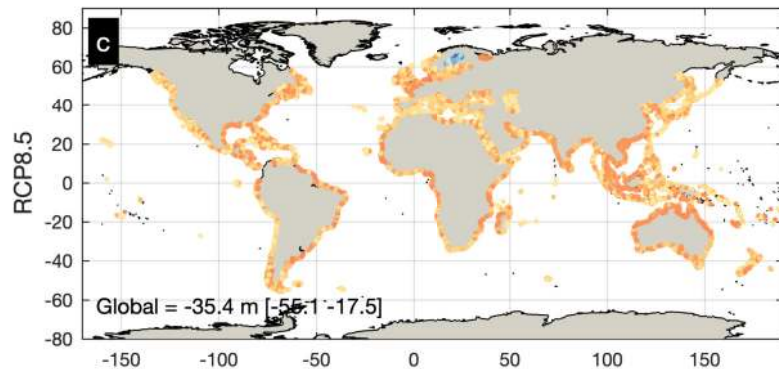
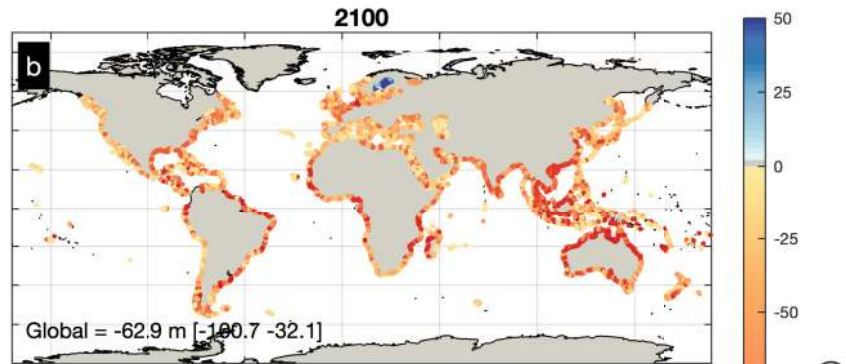
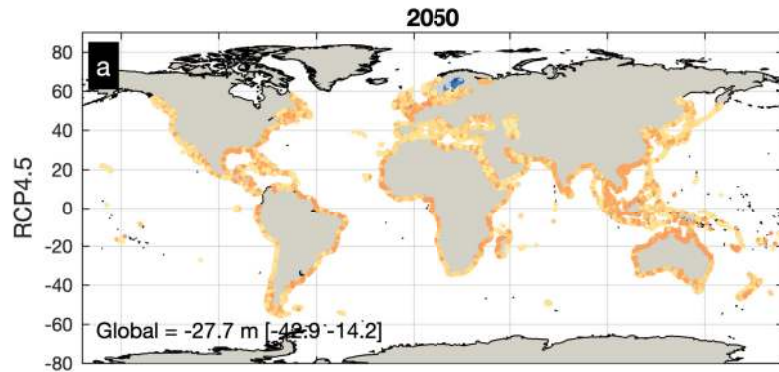
Ambient Change
  SLR Retreat
  RCP
  Shoreline Change





%sandy beaches with retreat over 100 m

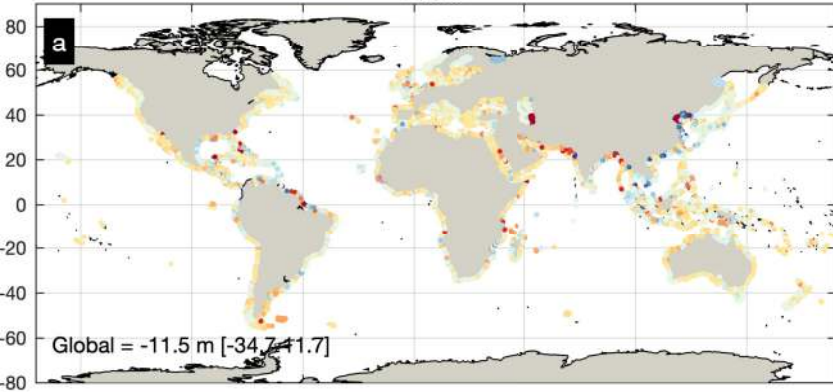




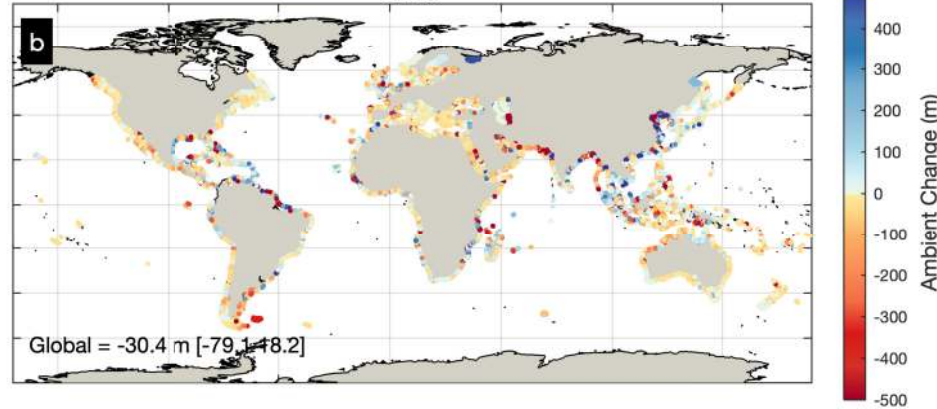
R (m)



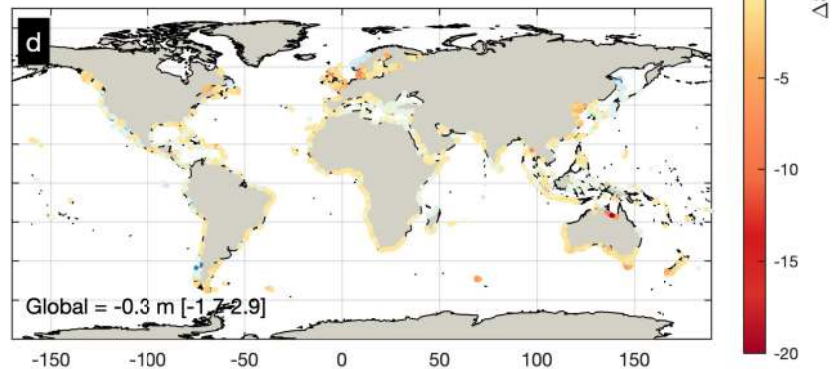
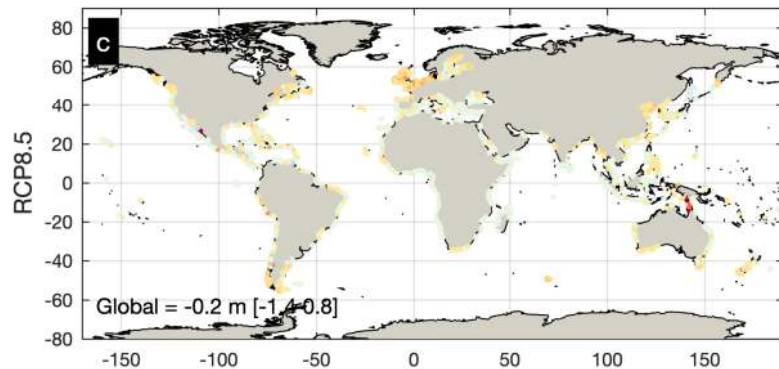
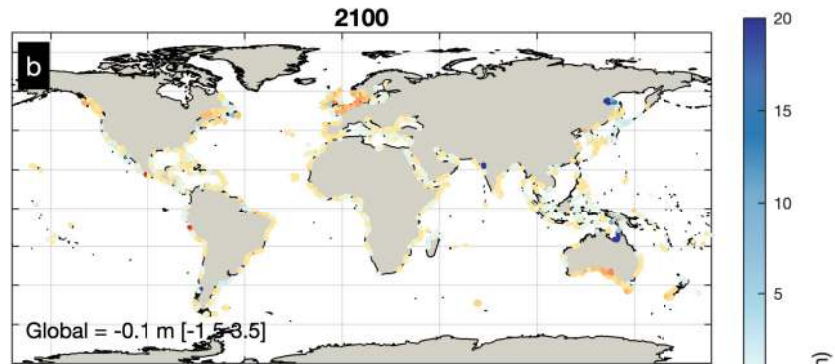
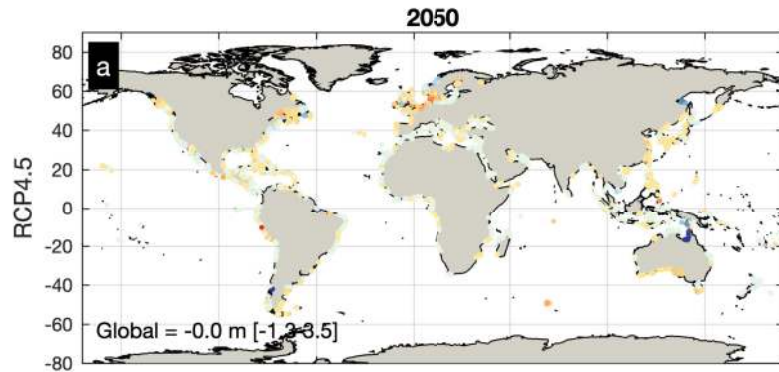
2050



2100



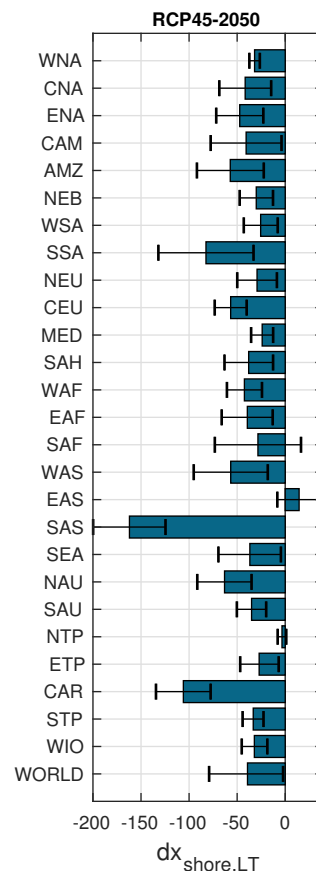
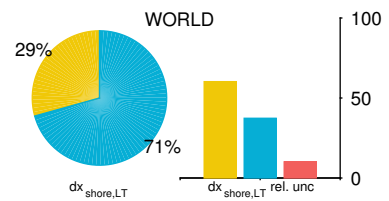
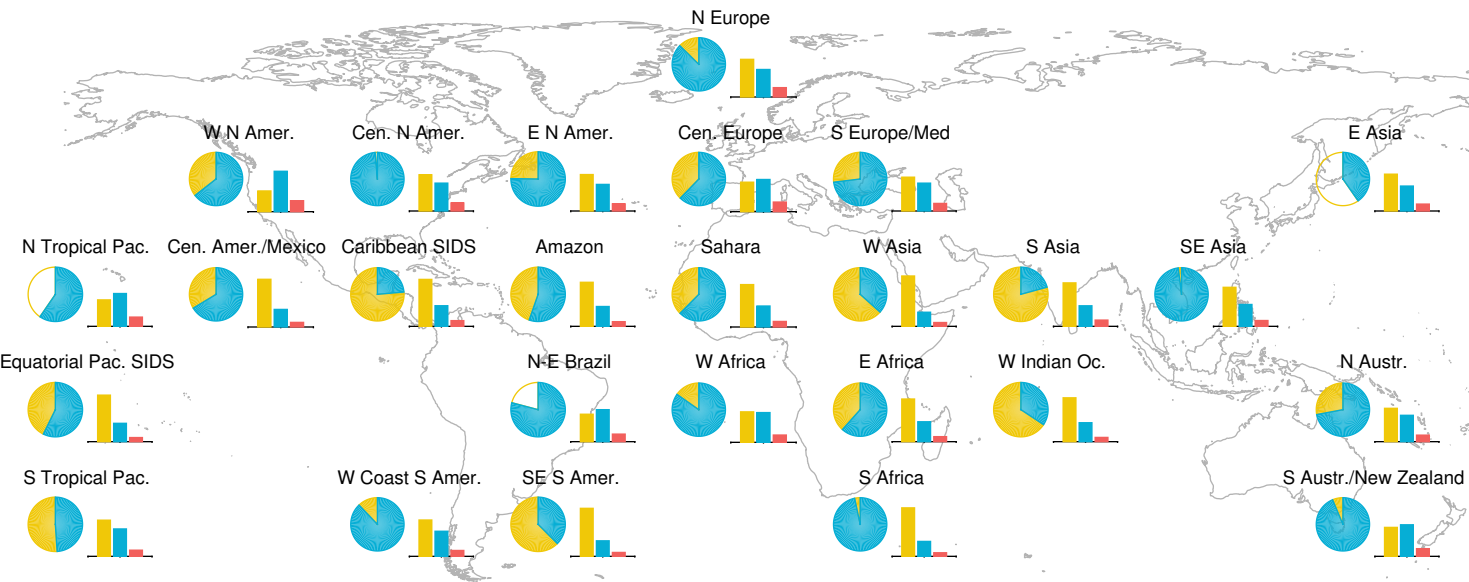




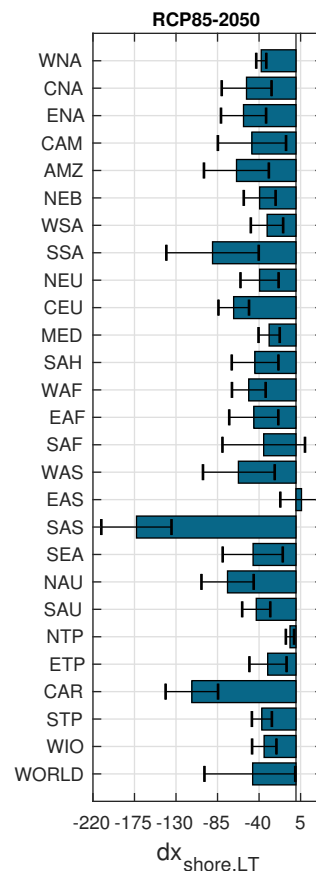
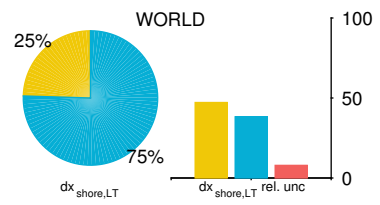
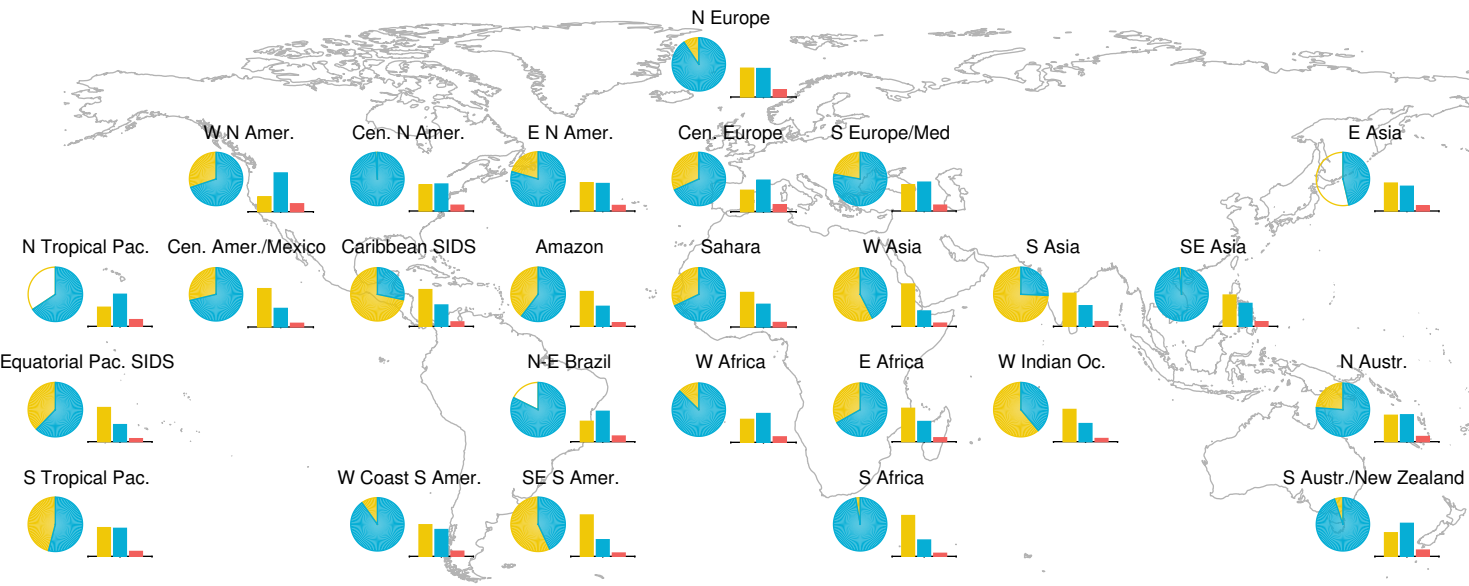
$\Delta S$  (m)



Ambient Change
  SLR Retreat
  RCP
  Shoreline Change

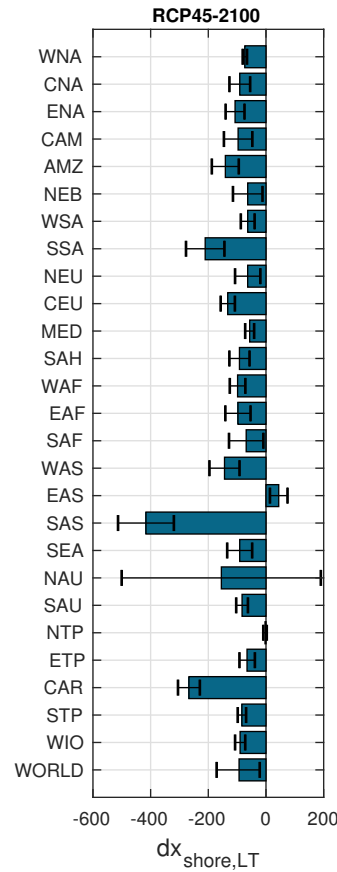
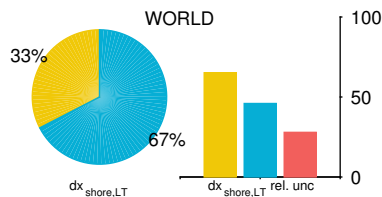
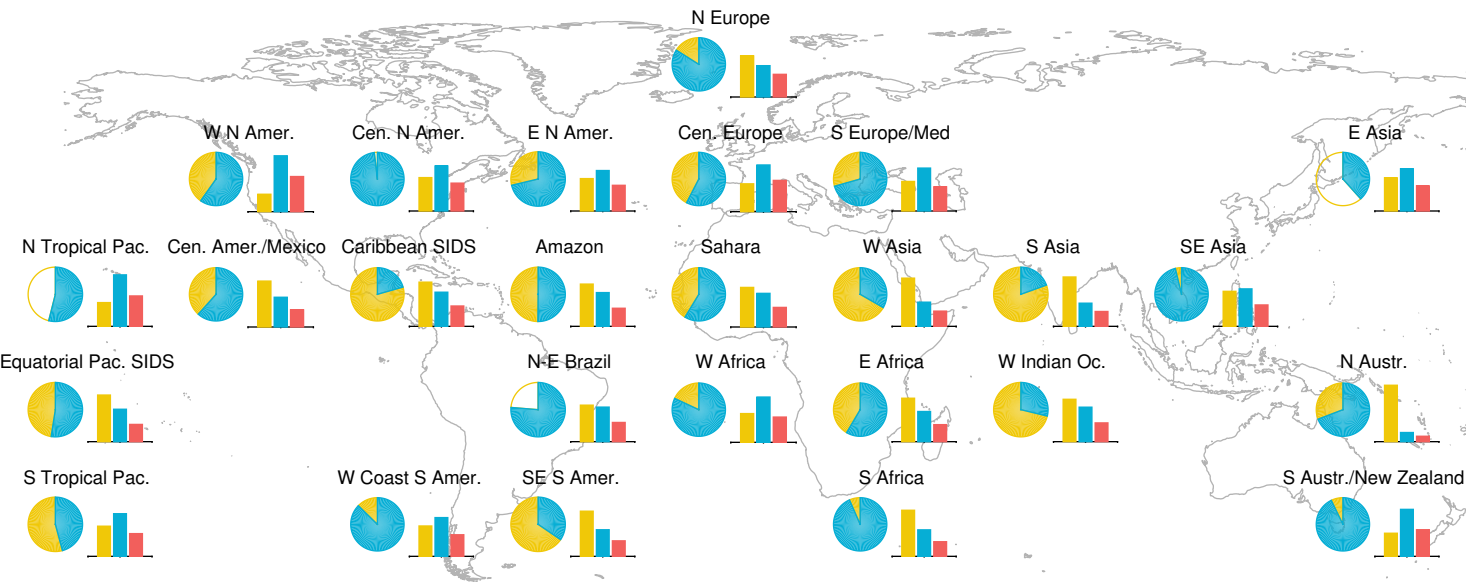


Ambient Change
  SLR Retreat
  RCP
  Shoreline Change





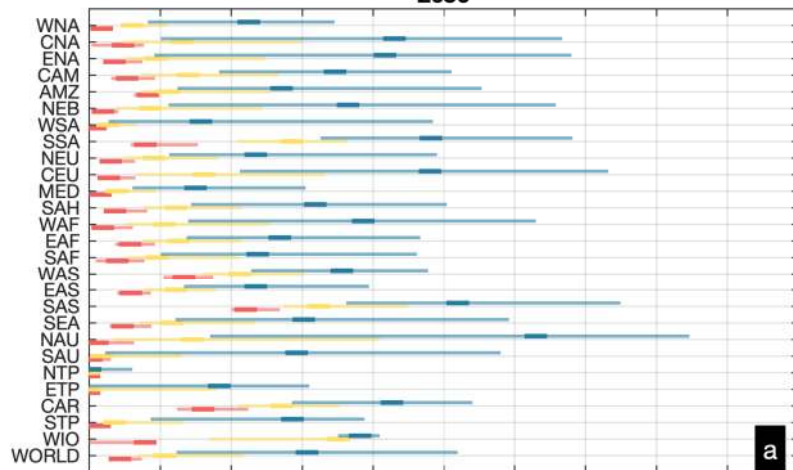
Ambient Change
  SLR Retreat
  RCP
  Shoreline Change



■  $dx_{shore} > 50$  m   
 ■  $dx_{shore} > 100$  m   
 ■  $dx_{shore} > 200$  m

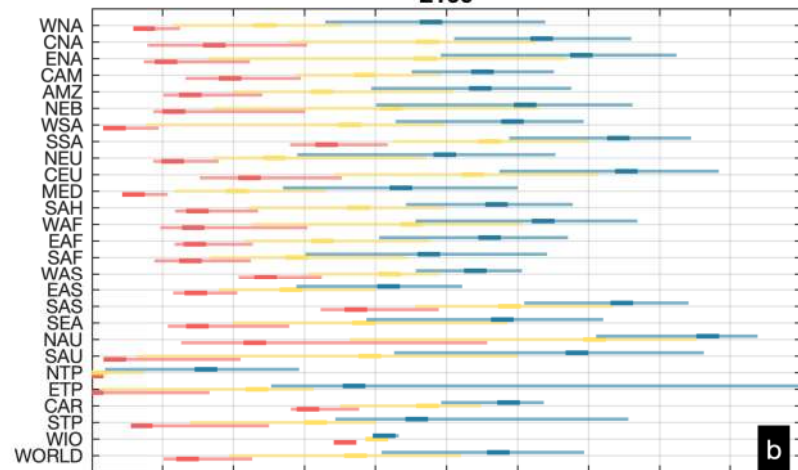
2050

RCP4.5



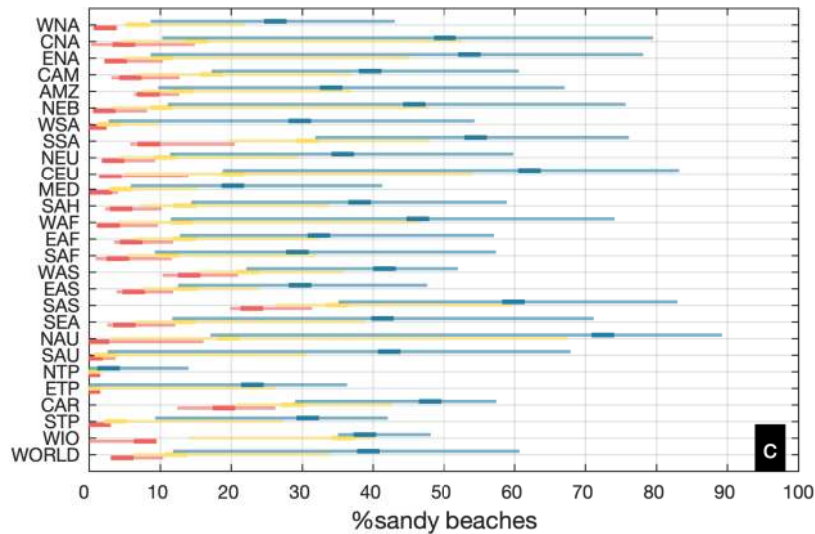
2100

RCP4.5

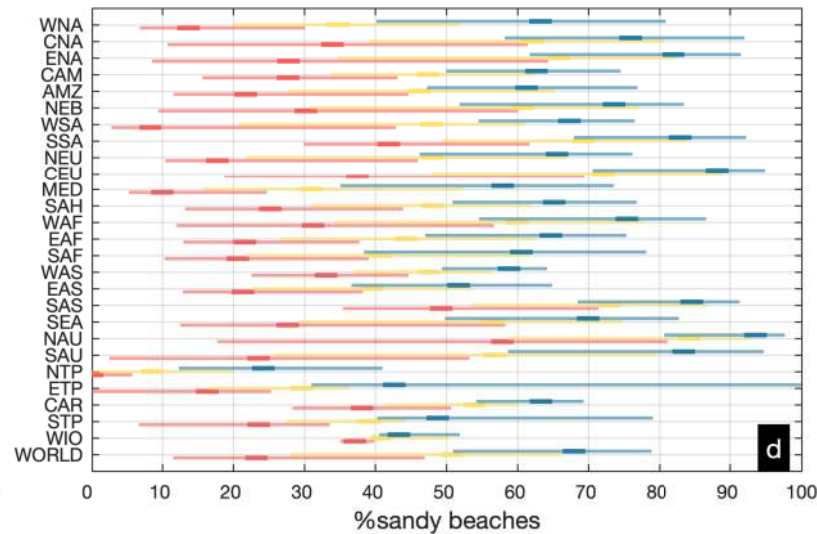


2050

RCP8.5



2100



■  $dx_{\text{shore}} > 50 \text{ m}$ 
■  $dx_{\text{shore}} > 100 \text{ m}$ 
■  $dx_{\text{shore}} > 200 \text{ m}$

